

КРАТКИЕ СООБЩЕНИЯ ОИЯИ

JINR RAPID COMMUNICATIONS

2[76]-96

-	Analytic QCD Running Coupling	
	with Finite IR Behaviour	
	and Universal $\overline{\alpha}_s(0)$ Value	
_	and Universal (s(0) Value	
	Quark Condensate	
	the Interacting Pion-Nucleon Medium	in
	at Finite Temperature	
	and Baryon Number Density	
_		
	$\gamma - \pi^0$ Discrimination	
	with a Shower Maximum Detector	
	Using Neural Networks	
	for the Solenoidal Tracker at RHIC	
	Off-Specular Neutron Reflection	
	from Magnetic Media	
	with Nondiagonal Reflectivity Matrices	
	Molecular Cytogenetics	
	of Radiation-Induced Gene Mutations	
	of Radiation-Induced Gene Mutations in Drosophila Melanogaster	

Издательский отдел ОИЯИ

ДУБНА

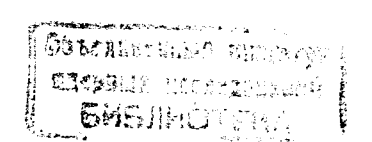


Объединенный институт ядерных исследований Joint Institute for Nuclear Research

2[76]-96

KPATKUE СООБЩЕНИЯ ОИЯИ JINR RAPID COMMUNICATIONS

Дубна 1996



ОГЛАВЛЕНИЕ CONTENTS

D.V.Shirkov, I.L.Solovtsov

Analytic QCD Running Coupling with Finite IR Behaviour and Universal $\overline{\alpha}_s(0)$ Value
Д.В.Ширков, И.Л.Соловцов Аналитическая бегущая константа связи КХД
с конечным ИК поведением
и универсальное значение $\overline{\alpha}_s(0)$ 5
T.I.Gulamov
Quark Condensate
in the Interacting Pion-Nucleon Medium
at Finite Temperature and Baryon Number Density
Т.И.Гуламов
Кварковый конденсат
во взанмодействующей пион-нуклонной среде
при конечной температуре и барионной плотности11
G.L.Gogiberidze, R.R.Mekhdiyev
$\gamma - \pi^0$ Discrimination
with a Shower Maximum Detector
Using Neural Networks for the Solenoidal Tracker at RHIC
Г.Л.Гогиберидзе, Р.Р.Мехтиев
Распознавание $\gamma-\pi^0$
в детекторе максимума ливня
для эксперимента STAR на колландере RHIC17
D.A.Korneev, V.I.Bodnarchuk, V.K.Ignatovich
Off-Specular Neutron Reflection from Magnetic Media
with Nondiagonal Reflectivity Matrices
Д.А.Корнеев, В.И.Боднарчук, В.К.Игнатович
Незеркальное отражение нейтронов от магнитных сред
с нелизгональными матринами отражения 25

I.D.Alexandrov, M.V.A. exandrova, I.L.Lapidus, A.L.Karpovsky	
Molecular Cytogenetics	
of Radiation-Induced Gene Mutations	
in Drosophila Melanogaster	
И.Д.Александров, М.В Александрова, И.Л.Лапидус, А.Л.Карповский	
Молекулярная цитогенетика	
радиационно-индуцированных геиных мутаций	
v Drosophila malanagastar	3′

. .

УДК 539.12.01

ANALYTIC QCD RUNNING COUPLING WITH FINITE IR BEHAVIOUR AND UNIVERSAL $\bar{\alpha}_s(0)$ VALUE

D.V.Shirkov, I.L.Solovtsov

As is known fom QED, a possible solution to the ghost-pole trouble can be obtained by imposing the Q^2 -analyticity imperative. Here, the pole is compensated by the α nonanalytic contribution that results in finite coupling renormalization.

We apply this idea to QCD and arrive at the Q^2 analytic $\overline{\alpha}_s(Q)$. This solution corresponds to perturbation expansion, obeys AF and, due to nonperturbative contribution, has a regular İR behaviour. It does not contain any adjustable parameter and has a finite IF limit $\overline{\alpha}_s(0)$ which depends only on group symmetry factors.

In the one-loop approximation it is equal to $4\pi/\beta_0 \simeq 1.40$ and turns out to be surprisingly stable with respect to higher order corrections. On the other hand, the IR be aviour of our new analytic solution agrees with recent global low energy experimental estimates of $\overline{\alpha}_s(Q^2)$.

The investigation has been performed at the Bogoliubov Laboratory of Theoretical Physics, JINR.

Аналитическая бегущая константа связи КХД с конечным ИК поведением и универсальное значение $\overline{\alpha}_s(0)$

Д.В.Ширков, И.Л.Соловцов

Как известно из КЭД, возможное решение проблемы призрачного полюса может быть получено наложением условия аналитичности по Q^{-2} . При этом полю: компенсируется выражением, неаналитичным по α , которое приводит также к конечной перенормировке заряда.

Мы используем эту идею для случая КХД и получаем для $\overline{\alpha}_s(Q)$ аналитическое выражение. Это решение обладает свойством асимптотической свободы, а его регулярность в инфракрасной области обязана непертурбативным вкладам. Оно не сс держит дополнительных параметров и в инфракрасной области имеет конечный предел $\overline{\alpha}_s(0)$, зависящий лишь от симметрийных факторов.

В однопетлевом приближении он равен $\overline{\alpha}_s(0) = 4\pi/\beta_0 \simeq 1.40$ и оказывается удивительно стабильным по отношению к высшим поправкам (тем самым схемно-инвариантным). Полученное аналитическое решение также согласуется с недавними интегральными экспериментальными оценками поведения $\overline{\alpha}_s(Q^2)$ в инфракрасной области.

Работа выполнена в Лаборатории теоретической физики им.Н.Н.Боголюбова ОИЯИ.

- 1. We recall first some results obtained in QED about 40 years ago. The QED effective coupling $\overline{\alpha}_s(Q^2)$, being proportional to the transverse dressed photon propagator amplitude, is an analytic function in the cut complex Q^2 plane and satisfies the Källen-Lehmann spectral representation. The «analytization procedure» elaborated in papers [1,2] consists of three steps:
- 1) Find an explicit expression for $\overline{\alpha}_{RG}(Q^2)$ in the space-like region by a standard RG improvement of perturbative input. Continue this expression to the time-like Q^2 domain.
- 2) Calculate the imaginary part of $\overline{\alpha}_{RG}(-Q^2)$ on the cut and define the spectral density $\rho_{RG}(\sigma, \alpha) = \text{Im } \overline{\alpha}_{RG}(-\sigma, \alpha)$.
- 3) Using the spectral representation with ρ_{RG} in the integrand, define an analytic $\overline{\alpha}_{re}(Q)$.

For one-loop massless QED, this procedure produces [2] an explicit expression (see Eq.(2.6) in Ref.[2] or analogous QCD Eq.(2) below) which has the following properties:

- a) It has no ghost pole;
- b) Considered as a function of α in the vicinity of the point $\alpha = 0$ it has an essential singularity of the exp $(-3\pi/\alpha)$ type;
- c) In the vicinity of this singularity for real and positive α it admits an asymptotic expansion that coincides with usual perturbation theory;
- d) It has a finite u traviolet asymptotic limit, $\overline{\alpha}(\infty, \alpha) = 3\pi$, which does not depend on the experimentally input value $\alpha \simeq 1/137$.

The same procedure in the two-loop massless QED approximation yielded [2] a more complicated expression with the same essential features.

2. To use the same technique in QCD one has to make two observations. First, since $\overline{\alpha}_s(Q^2)$ has to be defined via a product of propagators and a vertex function, validity of the spectral representation s not obvious. However, this validity has been established in Ref.[3] on the basis of analytic properties of the vertex diagrams. Second, for QCD with an arbitrary covariant gauge, the running of the coupling and gauge parameter are interconnected. For simplicity, we assume that the \overline{MS} scheme is used.

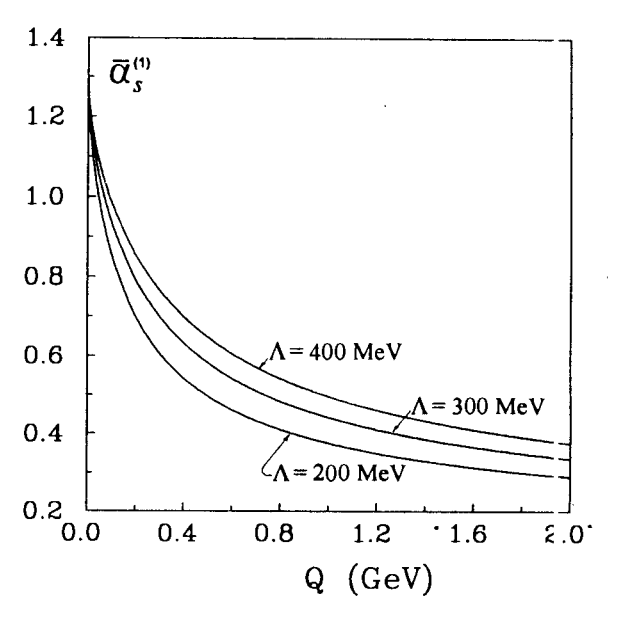
In the following we use the spectral representation in the nonsubtracted form

$$\overline{a}(Q^2) = \frac{\overline{\alpha}_s(Q^2)}{4\pi} = \frac{1}{\pi} \int_0^\infty \frac{\rho(\sigma, \Lambda) \, d\sigma}{\sigma + Q^2 - i\varepsilon} \,. \tag{1}$$

The usual massless one-loop RG approximation yields the spectral function

$$\rho_{RG}^{(1)}(\sigma \ \Lambda) = \frac{\pi}{\beta_0(l^2 + \pi^2)}, \quad l = \ln \frac{\sigma}{\Lambda^2}, \quad \beta_0 = 11 - \frac{2}{3} n_f.$$

Substituting $\rho_{RG}^{(1)}$ into spectral representation Eq.(1) we get



The behaviour of the analytic running coupling cons ant $\overline{\alpha}_s^{(1)}$ Eq.(2) versus Q at different Λ values

$$\overline{a}_{an,s}^{(1)}(Q^2) = \frac{1}{\beta_0} \left[\frac{1}{\ln Q^2 / \Lambda^2} + \frac{\Lambda^2}{\Lambda^2 - Q^2} \right], \tag{2}$$

where we have used the QCD scale parameter Λ . The «analytic» running coupling Eq.(2) has no ghost pole and its limiting value

$$\overline{\alpha}_{\rm s}^{(1)}(0) = 4\pi/\beta_0 \tag{3}$$

does not depend on A being a universal constant which depends on'y on group factors.

We have become accustomed to the idea that theory supplies us with a family of possible curves for $\overline{\alpha}_s(Q^2)$ and one has to choose the «physical one» of them by comparing with experiment. Here, in Eq.(2) the whole bunch of possible curves for $\overline{\alpha}_s(Q^2)$ corresponding to different Λ have the same limit at $Q^2=0$ as shown on the Figure. For $n_f=3$ it is equal to

$$\overline{\alpha}_s^{(1)}(0) = 4\pi/9 \simeq 1.396.$$
 (4)

Another feature of Eq.(2) is the fact that its correct analytic properties in the IR domain are provided by a nonperturbative contribution* like $\exp(-1/a\beta_0)$

^{*}The connection between « Q^2 analyticity» and « α nonperturbativity» has been discussed in Ref.[4].

To investigate the stability of the result, Eq.(4), with respect to the next loop corrections, we have considered the two-loop approximation to $\overline{\alpha}_c(Q^2)$ in the form

$$\overline{\alpha}_{RG}^{(2)} = \frac{1}{\beta_0 [L + b_1 \ln L]}, \quad L = \ln \frac{Q^2}{\Lambda^2}, \quad b_1 = \frac{\beta_1}{\beta_0^2}, \quad \beta_1 = 102 - \frac{38}{3} n_f$$

and

$$\rho_{RG}^{(2)}(\sigma, \Lambda) = \frac{I(l)}{\beta_0[R^2(l) + I^2(l)]}, \quad l = \ln \frac{\sigma}{\Lambda^2},$$

$$R(l) = l + b_1 \ln (\sqrt{l^2 + \pi^2}), \quad I(l) = \pi + b_1 \arccos \frac{l}{\sqrt{l^2 + \pi^2}}.$$
 (5)

The limiting two-loop value $\overline{\alpha}_s^{(2)}(0)$ is also specified only by group factors via β_0 and β_1 . Surprisingly, this value found by numerical calculation practically coincides with the one-loop result. For the \overline{MS} scheme in a three-loop approximation $\overline{\alpha}_s^{(3)}(0)$ changes by a few per cent. Thus, the value $\overline{\alpha}_s(0)$ is remarkably stable with respect to higher loop corrections and is practically independent of renormalization scheme.

3. To fix Λ we use the reference point $M_{\tau} = 1.78$ GeV with $\overline{\alpha}_s(M_{\tau}^2) = 0.33 \pm 0.03$ [5]. Corresponding solutiors $\overline{\alpha}_s^{(l=1,2,3)}(Q^2)$ are very close to each other for the interval of interest $Q^2 \leq 10$ GeV. For instance, at $Q^2 = 10$ GeV we have $\overline{\alpha}_s^{(1)}(10) \simeq \overline{\alpha}_s^{(2)}(10) = 0.267$, $\overline{\alpha}_s^{(3)}(10) = 0.255$. Here, again we used $n_f = 3$ as the average number of active quarks in the spectral censity. This seems to be reasonable in the IR region.

For a more realistic description of the evolution of $\overline{\alpha}_s(Q^2)$ in the Euclidean region 3 GeV < Q < 100 GeV, one should take into account heavy quark thresholds. Using the explicitly mass-dependent RG formalism [7] developed in the 50's, a «smooth matching» algorithm has been devised recently [6]. This can be given to correct analytic properties while incorporating heavy quark thresholds.

The idea that $\overline{\alpha}_s(Q^2)$ can be frozen at small momentum has been recently discussed in some papers (see, e.g., Ref.[8]). There seems to be experimental evidence indicating behaviour of this type for the QCD coupling. As the appropriate object for comparison with our theoretical construction we use the average

$$A(k) = \frac{1}{k} \int_{0}^{k} dQ \overline{\alpha}_{s}(Q^{2}, \Lambda).$$
 (6)

«Experimental» estimates for this integral are $A(2 \text{ GeV}) = 0.52 \pm 0.10 \text{ GeV}$ [9] and $A(2 \text{ GeV}) = 0.57 \pm 0.10 \text{ GeV}$ [10]. Our one-loop results in case Eq.(2) for A are summarized below for a few reference values of $\overline{\alpha}_s(M_\tau^2)$.

$\overline{\alpha}_s(M_{\tau}^2)$	0.34	0.36	0.38
A(2 GeV)	0.50	0.52	0.55

Note here that a nonperturbative contribution, like the second term in l.h.s. of Eq.(2), reveals itself even at moderate Q values by «slowing down» the velocity of the $\overline{\alpha}_s(Q^2)$ evolution. For instance, in the vicinity of c and b quark thresholds at Q=3 GeV it contributes about 4% which could be essential for the resolution of the «discrepancy» between DIS and Z_0 data for $\overline{\alpha}_s(Q^2)$.

4. We have argued that a regular analytic behaviour for $\overline{\alpha}_s(Q^2)$ in the IR region could be provided by nonperturbative contributions which can be considered as a sum of powers of Λ^2/Q^2 .

Probably, our most curious result is the stability of a «long-range intensity of strong interaction», $\overline{\alpha}_s(0)$, as well as the $\overline{\alpha}_s(Q^2)$ IR behaviour that turns out to agree reasonably well with experimental estimates.

On the other hand, the nonzero $\overline{\alpha}_s(0)$ value evidently contradicts the confinement property. To satisfy this, one should have

$$\overline{\alpha}_{s}(0) = 0$$

as it has recently been emphasized by Nishijima [11] in the context of the connection between asymptotic freedom (AF) and color confinement (CC).

It is possible to correlate this type of the IR limiting behaviour with the RG-improved perturbative input and Q^2 -analyticity by inserting a Castillejo-Ealitz-Dyson zero into our solution (see paper [12]). Such a generalyzed analytic solution will contain additional parameters. In this construction there is no evident relation between AF and CC. Here, CC is provided by nonperturbative contributions.

The authors would like to thank A.M.Baldin, A.L.Kataev and V.A.Rubakov for useful comments. Financial support of I.S. by RFBR (grant 96-02-16126-a) is gratefully acknowledged.

References

- 1. Redmond P. Phys. Rev., 1958, v.112, p.1404.
- Bogoliubov N.N., Logunov A.A., Shirkov D.V. Sov. Phys. JETP, 1959, v.37, p.805.
- 3. Ginzburg I.F., Shirkov D.V. Sov. Phys. JETP, 1965, v.49, p.335.
- 4. Shirkov D.V. Lett. Math. Phys., 1976, v.1, p.179.

- 5. Narison S. Phys. Lett., 1995, v.B361, p.121.
- Dokshitzer Yu.L., Shirkov D.V. Zeit. f. Phys., 1995, v.67, p.449;
 Shirkov D.V., Mikhailov S.V. Zeit. f. Phys., 1994, v.63, p.463.
- 7. Bogoliubov N.N., Shirkov D.V. Nuovo Cim., 1956, v.3, p.845.
- 8. Mattingly A.C., Stevenson P.M. Phys. Rev., 1994, v.D49, p.437.
- 9. Dokshitzer Yu.L., Webber B.R. Phys. Lett., 1995, v.B352, p.451.
- 10. Dokshitzer Yu.L., Khoze V.A., Troyan S.I. Phys. Rev., 1996, v.D53, p.89.
- 11. Nishijima K. Czech. J. Phys., 1996, v.46, p.1.
- 12. Kirzjnits D.A., Fainberg V.Ja., Fradkin E.S. Sov. Phys. JETP, 1960, v.38, p.239.

УДК 539.12.01

QUARK CONDENSATE IN THE INTERACTING PION-NUCLEON MEDIUM AT FINITE TEMPERATURE AND BARYON NUMBER DENSITY

T.I.Gulamov*

The chiral condensate in the interacting pion-nucleon system, $\langle \overline{q}q \rangle^*$, is it vestigated at finite temperature and density. The analysis has been done within the conventional hadron dynamics on the base of the Weinberg Lagrangian. At zero temperature and a finite nucleon density the interaction corrections increase the ratio $\langle \overline{q}q \rangle^*/\langle \overline{q}q \rangle_0$ at the level of $\simeq 10\%$. At finite value of the temperature, the thermalized pion population tends to compensate even this small effect, so that at high value of the temperature the in-medium chiral condensate becomes close to that in the free pion-nucleon gas.

The investigation has been performed at the Bogoliubov Laboratory of Theoretical Physics, JINR.

Кварковый конденсат во взаимодействующей пнон-нуклонной среде при конечной температуре и барионной плотности

Т.И.Гуламов

Киральный конденсат $\langle \overline{q}q \rangle^*$ исследуется во взаимодействующей пион-нуклонной среде при конечной температуре и плотности барионного заряда. Анализ проведен на основе лагранжиана Вайнберга. Учет взаимодействия приводит к слабому (порядка 10%) увеличению отношения $\langle \overline{q}q \rangle^*/\langle \overline{q}q \rangle_0$ при нулевой температуре. Однако при конечной температуре этот эффект компенсируется вследствие присутствия термализсванных пионов и их взаимодействия с нуклонными источниками. При высоких температ рах значение кирального конденсата во взаимодействующей среде почти не отличается от его значения в идеальном газе.

Работа выполнена в Лаборатории теоретической физики им.Н.Н.Боголюбова ОИЯИ.

I. Introduction

The investigation of hadron properties in the hot and dense nuclear matter is an important and interesting problem of the modern nuclear physics. Very likely, the effective hadronic parameters, the mass or decay width, could differ significantly from their values in the free space, depending on the temperature and density of the environment.

^{*}Physical and Technical Institute of the Uz.A.S., 700084, Tashkent, Uzbekistan.

Furthermore, the critical phenomena, such as formation of the quark-gluon plasma and the chiral symmetry restoration, are expected to occur in the extremely hot and dense matter.

One of the modern and widely used methods to study the in-medium effects is the QCD Sum Rules (QCD SR) [1], extended to the case of finite temperature and density [2]. While being successful in describing the hadron properties in free space, the QCD SR approach is also believed to be a useful tool for the theoretical investigation of hadron spectra in hot and dense nuclear matter. The reliable way is to describe the medium-nonaffected short-range dynamics in terms of quark and gluon degrees of freedom, while the long-range and medium-sensitive dynamics is described by introducing the temperature- and density-dependent in-medium condensates $\langle \bar{q}q \rangle^*$, $\langle G^{\mu\nu}G_{\mu\nu}\rangle^*$, etc. It has been made, for example, in Ref.[3], where the authors have evaluated, as input of the Sum Rule, the expectation values of quark and gluon operators taken over the states of the free pion gas at finite temperature. That scheme is reasonable for the investigation of hadron properties at relatively low temperatures and/or densities, whereas for a highly compressed and heated matter, the free gas approximation is certainly not relevant. To extend the consideration to higher values of the temperature and density, it is necessary to evaluate the thermal averages of the QCD operators in a strongly interacting system.

This problem is not new, in fact. The chiral condensate $\langle \overline{q}q \rangle^*$ in the hadronic medium at finite baryon number density was investigated in Refs.[4]. Another case, the interacting pion gas at finite temperature, was considered in Ref.[5]. In the present work, we study one more possibility, the interacting pion-nucleon gas at finite temperature and baryon number density, and evaluate the thermal average of the operator $\overline{q}q = \overline{u}u + \overline{d}d$, using the conventional hadron dynamics.

II. The Model

According to the Feynman-Hellmann theorem, the in-medium quark condensate is related to the free energy density (thermodynamical potential) $\Omega(T, \mu)$

$$\langle \overline{q}q \rangle^* = \frac{\partial}{\partial m_q} \Omega(T, \mu),$$

where m_q is the current quark mass. This form may be rewritten so as to separate the vacuum and matter pars:

$$\langle \overline{q} \gamma \rangle^{\bullet} = \frac{\partial}{\partial m_q} \Omega(0, 0) + \frac{\partial}{\partial m_q} (\Omega(T, \mu) - \Omega(0, 0)) \equiv$$

$$\equiv \langle \overline{q} q \rangle_0 + \frac{\partial}{\partial m_q} \Delta \Omega(T, \mu). \tag{3.1}$$

We'shall calculate the quantity $\Delta\Omega(T, \mu) \equiv \Omega(T, \mu) - \Omega(0, 0)$ within the conventional hadron dynamics. Therefore, $\Delta\Omega(T, \mu)$ explicitly depends on the effective hadron parameters (masses and coupling constants) rather than on the quark mass m_q . This means that to calculate the quark-mass derivative, one should employ the «chain rule» [4]:

$$\frac{\partial}{\partial m_q} \to \frac{\partial M_N}{\partial m_q} \frac{\partial}{\partial M_N} + \frac{\partial m_\pi^2}{\partial m_q} \frac{\partial}{\partial m_\pi^2} + \frac{\partial g_\pi}{\partial m_q} \frac{\partial}{\partial g_\pi} + \dots$$

Neglecting the dependence of the nucleon-meson couplings on the current quark mass, one can write:

$$\langle \overline{q}q \rangle^* = \langle \overline{q}q \rangle_0 + \left(\alpha_N \frac{\partial}{\partial M_N} + \alpha_\pi \frac{\partial}{\partial m_\pi^2} \right) \Delta \Omega^*(T, \mu) =$$

$$= \langle \overline{q}q \rangle_0 + \alpha_N \Delta \langle \overline{N}N \rangle^* + \alpha_\pi \frac{1}{2} \Delta \langle \pi_a^2 \rangle^*. \tag{3.2}$$

where the symbol $\Delta \langle Q \rangle^*$ stands for a matter contribution to the statistical average $\langle Q \rangle^*$ (so that $\Delta \langle Q \rangle^* \to 0$ as $T \to 0$, $\mu \to 0$), and N(N) and π_a are the nucleon and pion field operators, respectively. The coefficients $\alpha_{N,\pi}$ are defined by

$$\alpha_{N} = \frac{\partial M}{\partial m_{a}} = \langle N | \overline{q}q | N \rangle, \qquad \alpha_{\pi} = \frac{\partial m_{\pi}^{2}}{\partial m_{a}} = \langle \pi | \overline{q}q | \pi \rangle,$$

and can be found by using the Gell-Mann-Oakes-Renner (GMOR) relation [6] and the definition of the nucleon Σ_N -term [2,3,7]:

$$\alpha_N = -\frac{\Sigma_N}{f_\pi^2 m_\pi^2} \langle \overline{q}q \rangle_0, \qquad \alpha_\pi = -\frac{1}{f_\pi^2} \langle \overline{q}q \rangle_0.$$

The final expression of the ratio $R_{\overline{q}q} \equiv \langle \overline{q}q \rangle^* / \langle \overline{q}q \rangle_0$ reads:

$$R_{\overline{q}q} = 1 - \frac{\Sigma_N}{f_{\pi}^2 m_{\pi}^2} \Delta \langle \overline{N}N \rangle^* - \frac{1}{2f_{\pi}^2} \Delta \langle \pi_a^2 \rangle^*. \tag{3.3}$$

To calculate the «matter» parts of the averages $\langle \overline{N}N \rangle^*$ and $\langle \pi_a^2 \rangle^*$, we employ the Weinberg Lagrangian [8] that successfully combines the chiral symmetry predictions with low-energy $\pi - N$ phenomenology [9]. In this paper, we restrict ourselves to the second order in interaction and keep terms up to the third order in hadronic densities and their derivatives. The relevant piece of the Weinberg Lagrangian is of the type:

$$\mathcal{L}_{\text{int}} = \mathcal{L}_{1} + \mathcal{L}_{2} + \mathcal{L}_{3},$$

$$\mathcal{L}_{1} = \frac{g_{\pi}}{2M_{N}} \overline{N} \gamma^{5} \gamma^{\mu} \tau N \partial_{\mu} \pi, \qquad \mathcal{L}_{2} = \frac{i}{4f_{\pi}^{2}} \overline{N} \gamma^{\mu} \tau (\pi \times \partial_{\mu} \pi) N,$$

$$\mathcal{L}_{3} = \frac{-g_{N}}{8M_{N} f_{\pi}^{2}} \overline{N} \gamma^{5} \gamma^{\mu} \tau N \pi^{2} \cdot \partial_{\mu} \pi. \tag{3.4}$$

While performing the calculations, we neglect antiparticle states in the nucleon propagator. In this connection, we use the nonrelativistic reduction of the interaction vertices, given in the textbook [10].

III. Numerical Results and Discussion

For the numerical computation, we use the value of the sigma-term $\Sigma_N = 46$ MeV and $g_{\pi}^2/(4\pi) = 14.3$. Note that the $\Delta \langle \overline{NN} \rangle^*$ average in (3.3) is the scalar nucleon density, which in the nonrelativistic limit is reduced to the nucleon number density. Since we treat the nucleon density ρ as an independent variable, we replace the $\Delta \langle \overline{NN} \rangle^*$ by ρ and concentrate on the evaluation of the $\Delta \langle \pi_n^2 \rangle^*$.

Let us first consider the zero temperature limit, when the thermalized pions disappear and the interaction exhibits itself in the nucleon-nucleon correlations. The diagram giving

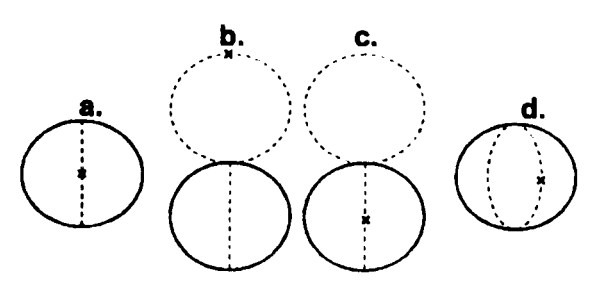


Fig. 1. The interaction corrections contributing to the ratio $\langle \bar{q}q \rangle^{*}/\langle \bar{q}q \rangle_{\rm vac}$. Solid and dashed lines denote nucleons and pions, respectively, and the cross denotes the operator insertion

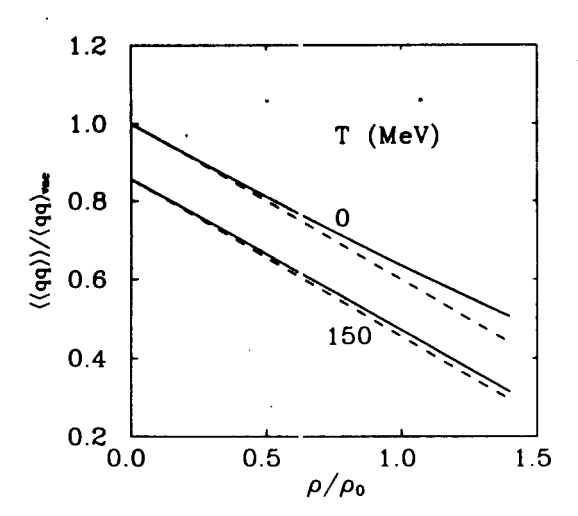


Fig.2. Density dependence of the ratio $\langle \bar{q}q \rangle^{\bullet}/\langle \bar{q}q \rangle_{\rm vac}$ at the different values of the tenperature. The dotted line is the ideal gas contribution and the solid line is the result of the full calculations

contribution at T = 0 is shown in Fig.1 (a), and represents the $\overline{q}q$ content of the exchanged pions. The numerical result at T = 0 is displayed in Fig.2 (upper curves), where the dashed line represents the ideal gas contribution and the solid line is the result of the complete calculation. Our result is in agreement with that of Ref. [11], where it was obtained from the calculation of the exchange Fock energy in the static approximation. Exchanged pions effectively grow the total in-medium value of the chiral condensate, but this correction is rather small and at the saturation density ρ_0 it does not exceed 10% of the ideal gas contribution.

The result at $T=150~{\rm MeV}$ is represented by the lower curves in Fig.2. It is seen from the figure that at a high value of temperature the interaction effect becomes even more weak. Recall that the contribution originated from the thermalized pion population is regulated mostly by the temperature. The positive contribution from diagram (a) is partially compensated by the contribution of diagrams (b, c), which is expected from the comparison of \mathcal{L}_1 and \mathcal{L}_3 (3.4). Other terms originated from the $NN\pi\pi$ interaction (\mathcal{L}_2 in (3.4) and diagram (d) in Fig.1)

give a positive contribution, thus effectively increasing the total in-medium content of $\langle \overline{qq} \rangle^*$. Despite these terms, the resulting behaviour of the chiral condensate in the interacting pion-nucleon medium at finite temperature and density is decreasing in shape.

We would like to mention the important role of other hadronic degrees of freedom which are not included into the present consideration. Inclusion of other types of N-N interaction (e.g., the repulsive vector-meson exchange) might alter the final results, but this question is beyond the scope of the present paper.

IV. Summary

In summary, we have estimated the chiral condensate $\langle \overline{q}q\rangle^*$ in the interacting pion-nucleon matter at finite temperature and baryon number density. The calculations are performed on the base of the conventional hadron dynamics up to the second order in interaction and the third order of hadronic densities and their derivatives. At zero temperature and of a finite nucleon density the interaction corrections slightly increase the ratio $\langle \overline{q}q\rangle^*/\langle \overline{q}q\rangle_0$. However, at finite temperature this effect is compensated by the contribution originated from the thermalized pions and their interaction with nucleon sources. This compensation is a consequence of the dynamics, based on the chiral symmetry.

Note that our results might be altered in a more realistic description. Namely, other light mesons, as well as delta isobars in the baryonic sector, should be included into consideration within conventional hadron dynamics based on the chira symmetry. Nevertheless, relying on the present schematic model we are able to figure out hints for interesting phenomena originatd from the finite temperature effects.

Acknowledgements

Useful discussions with Prof. A.I.Titov are greatly acknowled ged. The author also thanks D.A.Mirkarimov for helpful recommendations on the computational side.

References

- 1. Shifman M.A., Vainstein A.I., Zakharov V.I. Nucl. Phys. B, 1979, v.147, p.345.
- Bochkarev A.I., Shaposhnikov M.E. Nucl. Phys. B, 1986, v.268, p.220;
 Drukarev E.G., Levin E.M. Prog. Part. Nucl. Phys. A, 1991, v.556, p.467;
 Adami C., Hatsuda T., Zahed I. Phys. Rev. D, 1991, v.43, p.321; see also Ref. [3].
- 3. Hatsuda T., Koike Y., Lee S.H. Nucl. Phys. B, 1993, v.374, p.221.
- Cohen T.D., Furnstahl R.J., Kreigel K. Phys. Rev. C, 1992, v.45, p.1881;
 Celenza L.S., Pantziris A., Shakin C.M., Sun W.D. Phys. Rev. C, 1992, v.45, p.2015;

Chanfray G., Ericson M. — Nucl. Phys. A, 1993, v.556, p.427; Lee G.O., Ko C.M. — Phys. Lett. B, 1994, v.338, p.118.

- 5. Bunatian G., Wambach J. Phys. Lett. B, 1994, v.336, p.290.
- 6. Gell-Mann M., Oakes R., Renner B. Phys. Rev., 1968, v.175, p.2195.
- 7. Adami C., Brown G.E. Phys. Rep., 1993, v.234, p.1.
- 8. Weinberg S. Phys. Rev. Lett., 1966, v.17, p.616; Phys. Rev. Lett., 1967, v.18, p.188; Physica A, 1979, v.96, p.327.
- 9. Baym G., Campbell D.K. «Chiral Symmetry and Pion Condensation». In: «Mesons in Nuclei, v.3, Hortlı Holland Publishing Company, 1979 and references therein.
- 10. Ericson T., Weise W. «Pions and Nuclei», Clarendon Press, Oxford, 1988.
- 11. The first paper listed in [4].

УДК 539.1.074

$\gamma-\pi^0$ DISCRIMINATION WITH A SHOWER MAXIMUM DETECTOR USING NEURAL NETWORKS FOR THE SOLENOIDAL TRACKER AT RHIC

G.L.Gogiberidze¹, R.R.Mekhdiyev²

This paper presents a modern approach to discriminate $\gamma - \pi^0$ particles in the RHIC STAR shower maximum detector using neural nets. At the initial energy of 30 GeV the rejection factor, approximately 6, has been obtained for π^0 .

The investigation has been performed at the Particle Physics Laborator, JINR.

Распознавание $\gamma - \pi^0$ в детекторе максимума ливня для эксперимента STAR на коллайдере RHIC

Г.Л.Гогиберидзе, Р.Р.Мехтиев

С использованием методики нейронных сетей в рамках пакета JETN Ξ T смоделировано разделение $\gamma - \pi^0$ в детекторе максимума ливня установки STAR. При г ачальной энергии частицы 30 ГэВ достигнуто шестикратное подавление π^0 по отношение) к γ -квантам. Работа выполнена в Лаборатории сверхвысоких энергий ОИЯИ.

1. Introduction

The application of software neural network for the pattern recognition and triggering tasks, is well known. Here we have used a standard back propagat on training algorithm following the JETNET package [1] to study the problem of discrimination between photons and neutral pions in the shower maximum detector (SMD) for the solenoidal tracker at RHIC (STAR Project) [2]. This problem is especially difficult at high energies when two electromagnetic showers initiated by photons from the π^0 decay are overlapped and appear as a single cluster in the apparatus.

This ivestigation was motivated by the needs of the STAR experiment for the γ and γ -jet physics, to determine the kinematics of the primary quark-gluon scattering. On the other hand, a clean sample of π^0 -mesons is important for QCD studies.

¹Permanent address: Institute of Physics, Georgian Academy of Sciences, GE-380077 Tbilisi, Georgia, e-mail:

²Permanent address: Institute of Physics, Azerbaijan Academy of Sciences, AZ-370143 Baku, Azerbaijan, e-mail: mehdiyev@sunse.jinr.dubna.su

It is also interesting to investigate the ability of the neural network to distinguish two particle types, and how this ability depends on the energy of primary particles.

2. Pattern Generat on

A sampling calorimeter constructed of lead and plastic scintillator layers, was chosen for electromagnetic end-c μ calorimater (EMCE) in STAR Project [2]. The shower maximum detector, a part of EMCE, is placed at a depth of $\sim 5X_0$, between two longitudinal segments of EMCE. Its purpose is to measure centroids and lateral profiles of the showers to help electrons and gamma quanta to be separated from π^0 .

To generate patterns for training and testing, 24 strips, 1.0 cm wide, placed in radial direction, were included to one tower of the EMCE instead of two active plates of shower maximum detector. The total width of the tower was about 30 cm. Particles were directed to the central part of the tower, which is rather large and covers half of the tower. For practical application we suggest that signal can be read out from all strips of the tower as well as from the strip that covers the halves of the neighbouring towers. The edge effects of the electromagnetic shower development have not been considered here.

In total, 9000 events of each particle type were generated, 3000 — at the energy of 10, 20, and 30 GeV, correspondingly; 2500 of each set of particles were used for training and 500 — for test purposes. These single particle events have been pulled through the detector using a STAR simulation program which is close to the official version.

SMD was placed between two longitudinal segments of EMCE.

The amount of material in front of the SMD was estimated as follows:

- 8.0 mm aluminum walls of time projection chamber (TPC);
- 12.7 mm aluminum front plate;
- five layers of EMCE: 5-mm-thick lead absorber plates and 4-mm-thick scintillator (Polystyrene) tiles;
 - 3.2-mm-thick aluminium box of the shower maximum detector.

The maximum value of the magnetic field was 0.5 T.

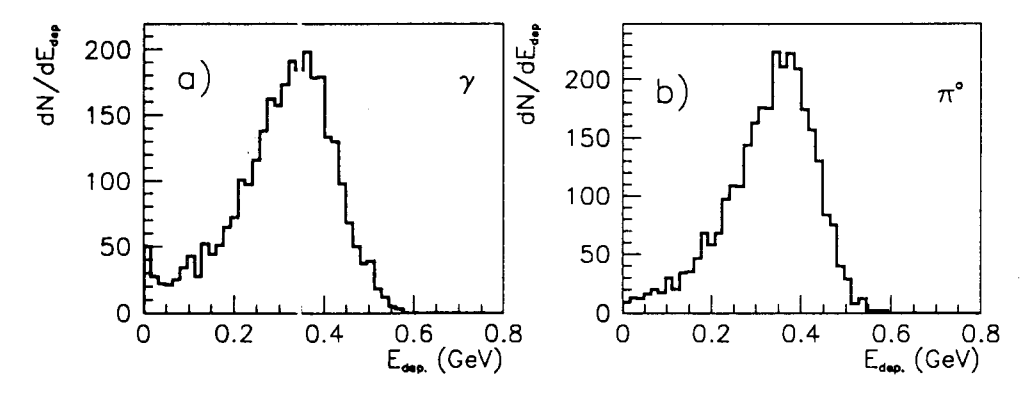
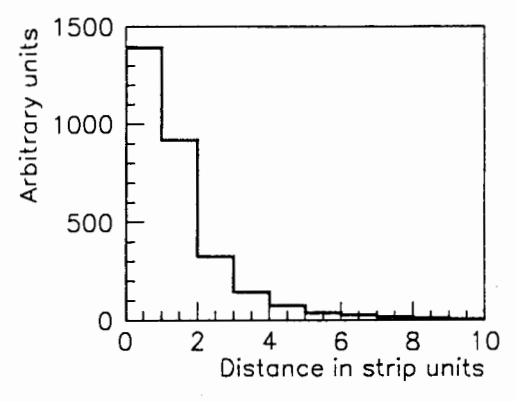


Fig.1. The distribution of the total energy deposition in shower maximum detector for γ (a) and π^0 (b) at 30 GeV



250 - 200 -

350

Fig.2. The distribution of the distance from the location of the SMD strip with maximum energy deposition

Fig.3. Asymmetry $R = \frac{(E1 - E2)}{E1 + E2}$ in the decay energies E1 and E2 of γ from π^0 decay

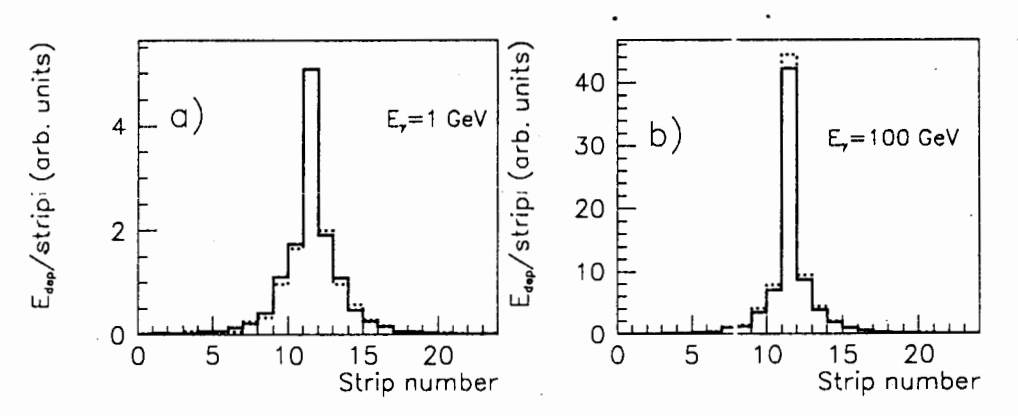


Fig.4. Profiles of e.m. shower in SMD initiated by 1 GeV (a) and 100 GeV (b) γ without (full line) and with (dotted line) magnetic field of 0.5 T

The distribution of the deposited energy in the SMD for incident γ (a) and π^0 (b), correspondingly, is presented in Fig.1. It is clearly seen that even for π^0 there is a non-zero probability that the deposited energy disappears from the first longitudinal segment of EMCE.

Let us enumerate possible cases when it is unachievable to resolve two photons from the π^0 decay:

- One of the photons is missed because it is outside the detector acceptance. Figure 2 shows the distribution of energy deposition depending on the distance from the location of the SMD strip having maximum energy deposition.
- One of the photons has a low energy and cannot be distingt ished from the noise. The curve presented in Fig.3 shows asymmetry $R = \frac{(E1 E2)}{E1 + E2}$ in the π^0 decay resulting in two γ -s with energies E1 and E2.

- One of photons does not give a significant energy deposition in the SMD due to statistic factors (γ does not convert before the SMD).
- Effective distance between two photons is small, compared with the transverse size of the electromagnetic shower.

The last effect strongly depends on the thickness of the matter before the SMD and the magnetic field which turns trajectories of the charged particles and therefore spreads out the electromagnetic shower. Figure 4 shows the averaged profiles of the e.m. shower in the SMD strip layers without (full line) and with (dotted line) magnetic filed of 0.5~T for γ with incident energy of 1 GeV (1) and 100~GeV (b), correspondingly.

Only these particles which give the energy deposition in the SMD not less than 40% on the average, are considered further. About 8% of events were rejected using this cut in the paper.

3. Network Training

The task to separate γ and π^0 is reduced to determining the correspondence between selection of the X_i input values and Y output values whose true meanings are known beforehand.

Our strategy was not to use sophisticated variables as, for example, in [3] but just the energy deposition in strip for input nodes. It is significant, that this method can be used not only for an off-line analysis, but also for a triggering, of course, with necessary hardware.

The architecture of the network employed in the present study is a conventional one, i.e., a network of the feed forward type with two hidden layers.

In this paper we do not intend to determine the best architecture, where the number of the hidden nodes is considered optimal. We have used two layers of hidden nodes. These results were obtained with the 24-16-8-1 architecture. The increase of the hidden nodes number does not improve the situation much, but dramatically rises the training time.

Due to the high number of connected weights in the neural network the principle of mirror symmetry has been used. We have prepared ordinary and «inverted» patterns with an equal probability, where strip number i was replaced by strip number 24 - i + 1.

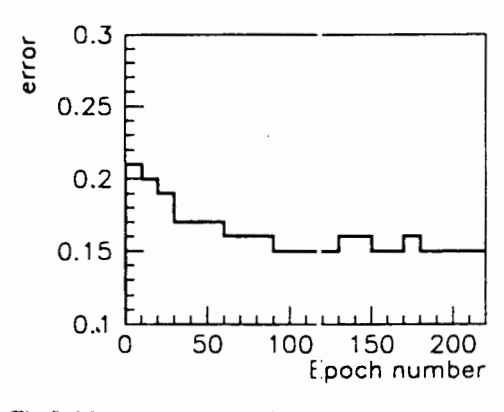


Fig. 5. Mean square error E vs. epoch number

This is done to meet the ordinary requirements for neural nets: the number of patterns should be more than the number of the connected weights by 10 times.

The network starts with random weights, the training vector (normalized energy deposited in strips) feeds into the network through; the output vectors o_i (dimensional in our case) are calculated and compared with target vector t. If the pattern is γ , then t is equal to 1, if not — t is equal to zero. When k events are presented to the network, the weights are updated by minimization of the summed square error E for all patterns k:

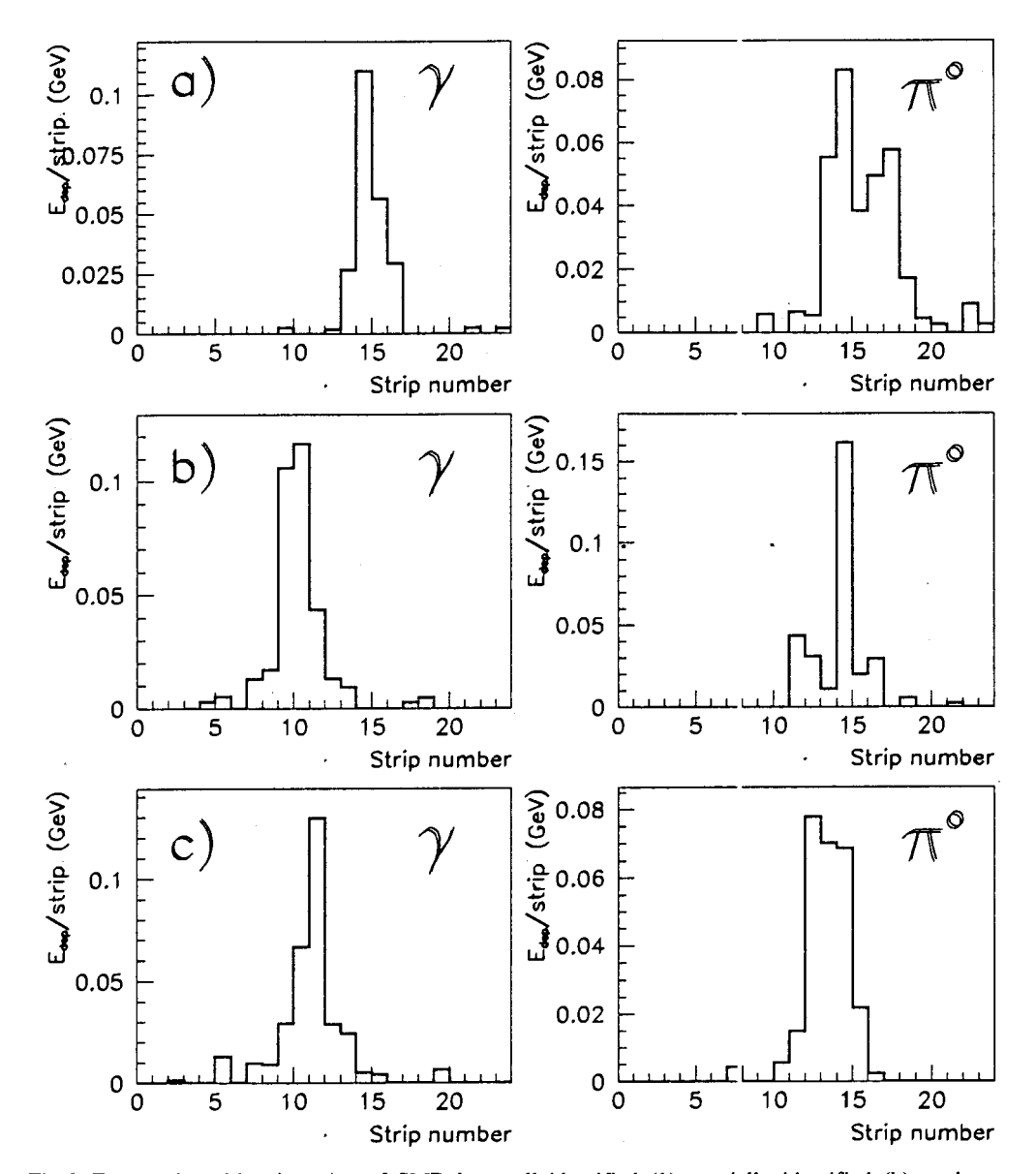


Fig.6. Energy deposition in strips of SMD by: well identified (1), partially identified (b), and poor identified (c) γ (left side) and π^0 (right side)

$$E = \frac{1}{2k} \sum_{k} (o_k - t_k)^2.$$
 (1)

Weights were updated using the Langevin learning procedure which includes the Gaussian noise (0.2 of learning rate in our training). This procedure was repeated every k events. Our choice was k = 10.

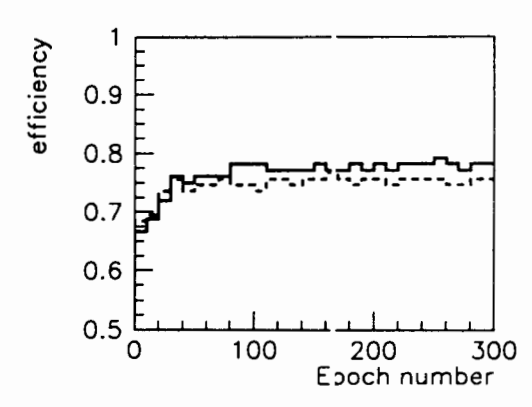


Fig. 7. Neural network response (threshold $\varepsilon = 0.5$) for training (solid line) and testing (dash line) sets in dependence on the epoch number

Presentation of the number of patterns equal to their quantity in the test set according to the adopted terminology is called epoch. The decreasing of a mean square error during the network training is shown in Fig.5. For each epoch the percentage of the correctly classified patterns is computed by means of threshold $\varepsilon = 0.5$, classifying an input as y, if the output is greater than E, and as pion — in another case. It must be emphasized that various & thresholds can be used for practical purposes. The neural net recognizes patterns using shapes of energy deposition in the SMD strips with different results: (a) well identified; (b) partially identified and (c) hardly or misidentified y and π^0 with the incident energy of 30 GeV (Fig.6).

The increase of network response (threshold $\varepsilon = 0.5$) for training and testing sets in dependence on the epoch number is presented in Fig.7. The difference illustrates adaptation of the neural net to the training set. This can be improved by a significant increase of the training set, but, at present, this way is costly due to CPU time.

4. Results

The set of test events used for checking the neural net response is completely independent of the training event set. Figure 8 presents the distribution of e.m. shower width for the events initiated by photons and pions of 10 GeV (a) and 30 GeV (b) initial energy. Shower width is defined as follows: $W = \frac{1}{2} \sum_{k} (R_k)^2 \times E_k$ for γ (solid line) and π^0 (dashed line), where R_k is the distance between the center of the shower and strip number k, E_k energy deposited in the strip. Using this information we can reject γ from π^0 for the 10 GeV initial energy, but for 30 GeV the difference is small. With about 10% of γ loss, the cut on the shower transverse size can reject only 45% of π^0 .

Figure 9 shows the output signal for showers initiated by γ and π^0 for the 10 GeV (a) and 30 GeV (b) initial energy, correspondingly. As is seen, at the initial energy of 30 GeV the neural network can reject about 66% of π^0 with γ losses less than 10%.

To determine a possib lity of improving the neural net response using a complementary information for 30 GeV events, we have combined the EMCE and the SMD information. Three additional input var ables have been used:

- Maximum energy in the tower of the first longitudinal part of EMCE divided by the total energy deposition in this first part;
- · The same for the second longitudinal part;

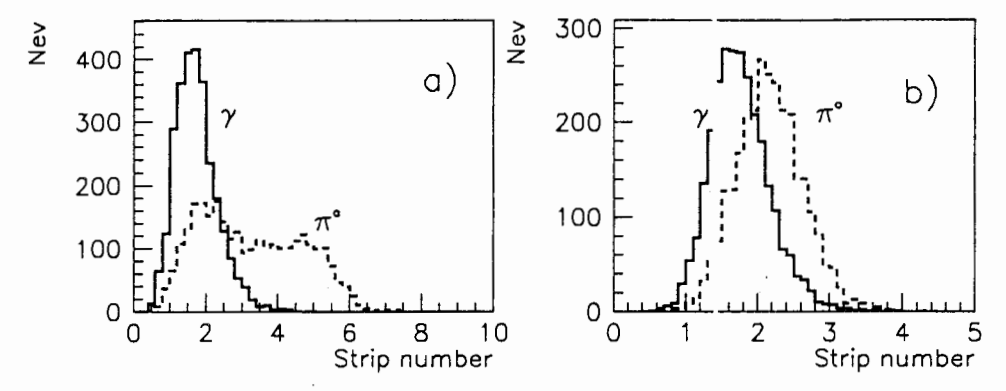


Fig. 8. Distribution of e.m. shower width, as defined in the text, for 10 CeV (a) and 30 GeV (b) initial energy

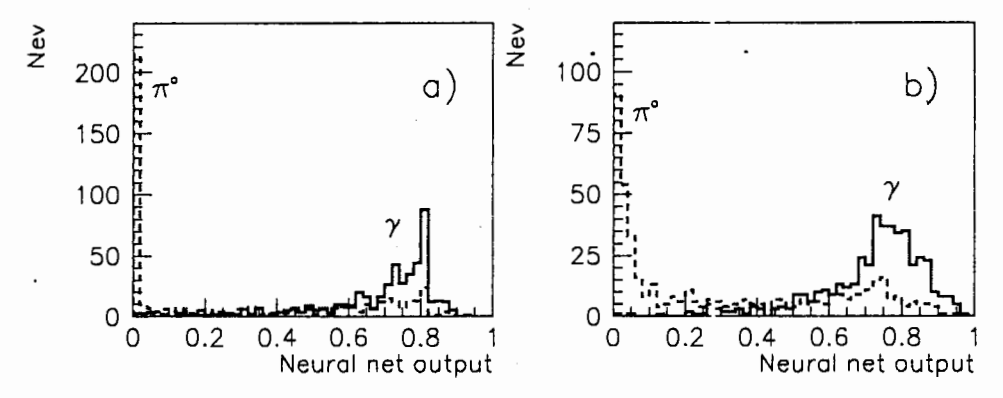


Fig. 9. Neural net output for γ (dashed) and π^0 (solid) of 10 GeV (a) and 30 GeV (b) initial energy

• Total energy deposition in the first longitudinal part is divided by the total energy deposition in the EMCE.

We have also rejected the events with a small energy value (10% in average) deposited in the second hidden layer (less than 1% of all events). The 27-20-10-1 architecture and large number of training epoch (5000) have been used. The discrimination results on $\gamma - \pi^0$ made in the neural net at the initial energy of 30 GeV are given in Fig.10.

Let us define the rejection factor as the ratio of the number of signal gone through some conditions — to the number of background events also gone through the same conditions. With losses of γ less than 50%, the rejection factor, approximately 6, for π^0 has been obtained.

In Ref. [3] it is written that with the energy increasing the relative efficiency of neural network algorithm for $\gamma-\pi^0$ separation is better, compared with other algorithms. In our investigation the efficiency of neural network algorithm does not deteriorate with the energy increase.

It should be also noted, that despite the fact that the use of the information from EMCE decreases the mean square error as defined in (1) from 0.14 to 0.12, still it does not

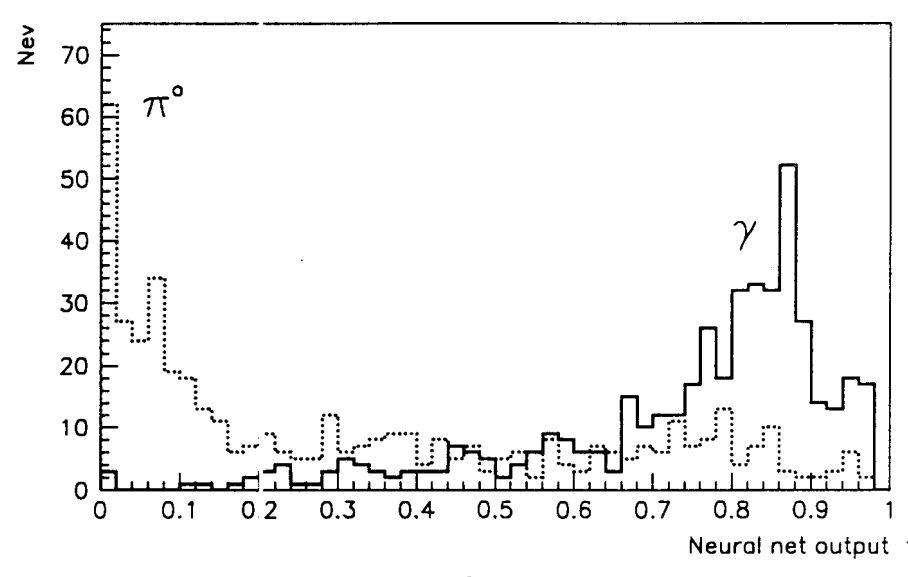


Fig. 10. Neural net output for γ (dashed) and π^0 (solid) with additional EMCE information

drastically improve $\gamma - \pi^0$ separation. This can be explained in the spirit of [4]. Let us consider the border patterns, those where the neural net output is close to the border between the classes, e.g., is about 0.5. Adaptation of the neural net on the training set happens due to the number of the border patterns in the training set approximately equal to the number of connected weights $\sim 10^3$. Additional training of the neural net on these border patterns (but independent of the initial training set) can improve the situation, but to generate the patterns requires huge CPU time resources.

5. Conclusion

Back propagation neural network is a powerful tool to study γ and π^0 separation in the STAR detector. Training and testing were performed with the Monte Carlo data. Results are presented for «poor» (one layer of strips) SMD choice. Rejection factor against π^0 equal to 6 at 53% γ -efficiency is achieved for the initial particle energies of 30 GeV.

References

- Lönnblad L., Peterson C., Rögnvaldsson T. Comput. Phys. Comm., 1992, v.70, p.167.
- 2. The Electromagnetic Calorimeter for the Solenoidal Tracker at RHIC, PUB-5380, p.4—40.
- 3. Babbage W., Thompson L. Nucl. Instr. and Meth., 1993, v.A330, p.482.
- 4. Peterson C., Rögnvaldsson T. CERN School of Computing, CERN 92-02, 1991, p.113.

Received on March 25, 1996.

УДК 538.97

OFF-SPECULAR NEUTRON REFLECTION FROM MAGNETIC MEDIA WITH NONDIAGONAL REFLECTIVITY MATRICES

D.A.Korneev, V.I.Bodnarchuk, V.K.Ignatovich

The reflection of neutrons from magnetic substances is described using the reflection matrix with nondiagonal, in general, matrix elements which determine neutron spin reverse. In external field the spin reverse is accompanied by changes of the neutron kinetic energy and reflection angle. The particular case of reflection from a magnetic mirror with magnetization noncollinear to the external field is considered. The probability of spir reverse and a deviation of reflection angles from the specular one are calculated. The experiment to observe this effect is described and its results are reported.

The investigation has been performed at the Laboratory of Neutro 1 Physics, JINR.

Незеркальное отражение нейтронов от магнитных сред с неднагональными матрицами отражения

Д.А.Корнеев, В.И.Боднарчук, В.К.Игнатович

Отражение нейтронов от магнитных сред описывается матрицей отражения с отличными от нуля, в общем случае, недиагональными компонентами, которые определяют вероятность переворота спина. Во внешнем поле переворот спина приводит к изменению кинетической энергии нейтрона и угла отражения. В работ: рассматривается частный случай отражения от магиитного зеркала, намагниченность к эторого непараллельна внешнему полю. Вычисляется вероятность переворота спина и вел ччина отклонения угла отражения от зеркального. Дано описание эксперимента и его результатов по наблюдению данного эффекта.

Работа выполнена в Лаборатории нейтронной физики ОИЯИ.

1. Introduction

Since the time of the first works by Hughes and Burgy [1] specular reflection has been used to polarize neutrons. With polarized neutrons one can investigate, for instance, magnetization profiles of films and multiayered systems [2—6]. It was pointed out [7—13] that reflection from films with noncollinear magnetic structures is more complicated than reflection from films with collinear ones. In noncollinear case the reflection is characterized by the reflection matrix:

$$\hat{R} = \begin{pmatrix} R_{++} & R_{+-} \\ R_{-+} & R_{--} \end{pmatrix}$$

with nonzero elements R_{+-} and R_{-+} . To measure all matrix elements in \hat{R} is the main goal of polarized neutron reflect ometry.

In the next section, the angular characteristics of reflection with spin-flip in external fields are considered. In the third section, the matrix elements of R and the intensities of constituent beams for the case of reflection from a magnetic mirror with magnetization noncollinear to the external field are calculated. In the fourth section, the experiment to observe the off-specular reflection is described.

2. Angular Splitting of the Reflected Beam

The reflection of neutrons from an interface in an external magnetic field can be off-specular (though coherent) if it is accompanied by spin flipping [7,9]. In general, the incident beam after reflection undergoes triple splitting, as shown in Fig.1. It contains the middle part which is specular and two side lobes which are off-specular and perfectly polarized. The intensities of the side lobes are determined by the matrix elements R_{+-} and R_{-+} of the matrix R and by incident beam polarization. If the incident beam is perfectly polarized, one of the side lobes vanishes. If the incident beam is nonpolarized, two side beams in weak external fields have almost equal intensities. The splitting of the beam takes place because of spin flipping, energy conservation and the conservation of components of neutron momentum parallel to the interface.

Let us denote $\mathbf{k} = (\mathbf{k}_{\parallel} \ \mathbf{k}_{\perp})$ the wave vector of the incident neutron with the \mathbf{k}_{\perp} , \mathbf{k}_{\parallel} being its normal and parallel to the surface components. In the external field **B** the neutron has the potential energy $- \epsilon r \mathbf{B}$, where **B** is measured in $h^2/2m\mu$ (m, μ) are the neutron mass

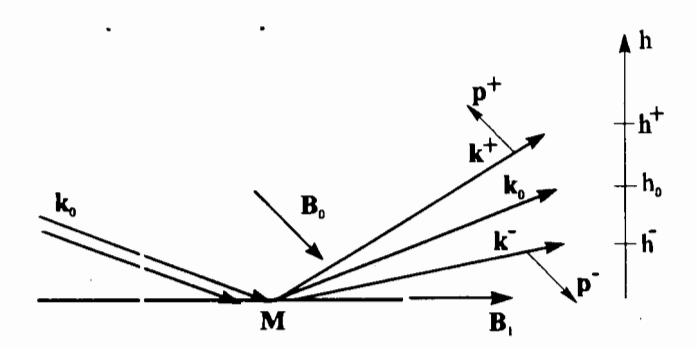
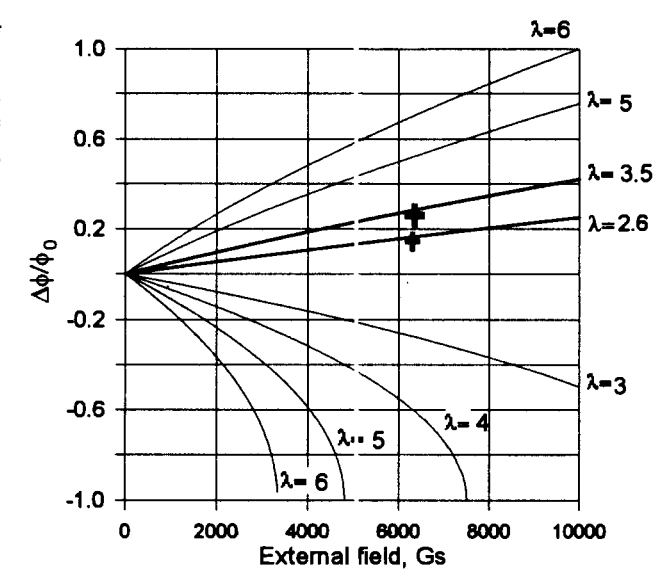


Fig. 1. Following the reflection from a magnetized mirror with the magnetization M noncollinear to the external magnetic field B_0 the nonpolarized incident neutron beam with a wave vector k_0 splits into three beams. Two off-specular beams with the wave vectors k^+ and k^- are ideally polarized. The splitting of the beam gives the distribution over height h of the reflected neutrons and it can be measured by a moving or a position sensitive detector

Fig. 2. The relative angular splitting of spin reversed beams in dependence on λ (in Angstroms) and the external magnetic field for $\phi_0 = 4.2$ mrd. The crosses are the experimental points (see Sec.4)



and magnetic moment, respectively) and σ are the Pauli matrices. On spin reverse the potential energy changes in magnitude by $\pm 2B$. Because of energy conservation it changes the kinetic energy: $k^2 \to k^2 \pm 2B$. In the reflection from an interface the components \mathbf{k}_{\parallel} , are also conserved. Thus the change of the kinetic energy means the change in the normal component \mathbf{k}_{\perp} : $k_{\perp} \to k_{\perp}^{\pm} = \sqrt{k_{\perp}^2 \pm 2B}$, and as a result leads to change in the reflection angle. It is not difficult to calculate the angular deviation of shifted beams. For a small grazing angle $\phi_0 = 10^{-2} + 10^{-3}$ we have

$$\frac{\Delta \phi^{\pm}}{\phi_0} = \frac{\Delta k_{\perp}^{\pm}}{k_{\perp}} = \sqrt{1 \pm 2B/k_{\perp}^2} - 1 = \sqrt{1 \pm 1.47 \cdot 10^{-10}} \cdot \overline{B_0 \lambda^2/\phi_0^2} - 1.$$

Here the neutron wavelength λ is measured in Angstroms; B, in Gauss; and ϕ_0 , in radians. The dependence of relative splitting $\Delta \phi^{\pm}/\phi_0$ on λ and B is shown in Fig.2.

If the external field is sufficiently large, spin reverse is forbidden for $\Delta \phi < 0$.

3. Matrix \hat{R}

Let us find the solution of the Schrödinger equation in the presence of the external magnetic field ${\bf B}_0$ and a magnetized reflecting mirror:

$$(\Delta - u\theta(z > 0) + \sigma \mathbf{B}(z) + k^2) \Psi = 0, \tag{3.1}$$

where u is an optical potential of the mirror, which is supposed to fill the half space z > 0, θ is a step function equal to unity when the unequality in its argument is satisfied and to zero in the opposite case,

$$\mathbf{B}(z) = \mathbf{B}_0 \theta(z < 0) + \mathbf{B}_1 \theta(z > 0),$$

and \mathbf{B}_1 is the magnetic induction of the mirror. We consider the case when \mathbf{B}_0 is unparallel to \mathbf{B}_1 . The solution is: $\psi(\mathbf{r}) = \exp(i\mathbf{k}_{\parallel} \mathbf{r}_{\parallel}) \xi(z)$, where

$$\xi(z) = \Theta(z < 0) \left[\exp \left(i \hat{k}_{\perp}^{\dagger} z \right) \xi_{0} + \left[\exp \left(- i \hat{k}_{\perp}^{\dagger} z \right) \hat{R} \xi_{0} \right] + \theta(z < 0) \exp \left(i \hat{k}_{\perp}^{\dagger} z \right) \hat{T} \xi_{0},$$
(3.2)

 \hat{R} , \hat{T} are reflection and transmission matrices, $\hat{k}_{\perp}^{\pm} = \sqrt{k_{\perp}^2 \pm \sigma B}$, $\hat{k}_{\perp}^{\prime \pm} = \sqrt{k_{\perp}^2 - u \pm \sigma B}$, and ξ is the spinor state of the incident particle. For simplicity in the following, we shall omit the subscript \perp .

Matching of the wave function at the interface z = 0 for arbitrary ξ_0 gives two equations for \hat{R} and \hat{T} :

 $\hat{I} + \hat{R} = \hat{T}, \qquad \hat{k}^{+}(\hat{I} - \hat{R}) = \hat{k}'^{+}.$

The solution of these equations can be represented as follows:

$$\hat{R} = (\hat{k}^+ + \hat{k}'^+)^{-1} (\hat{k}^+ - \hat{k}'^+), \qquad \hat{T} = (\hat{k}^+ + \hat{k}'^+)^{-1} 2\hat{k}^+$$

Here we shall consider in detail the matrix \hat{R} only:

It is possible to get rid of the matrices σ in the denominator by representing \hat{R} in the form

$$\hat{R} = (\hat{k}^{-} + \hat{k}')(\hat{k}^{+} - \hat{k}'^{+})/N \equiv \hat{A}/N, \tag{3.3}$$

where, N is the number and it is useful to calculate it as a matrix element:

$$N = \langle + \mid k^{+}k^{-} + \hat{k}'^{+} \hat{k}'^{-} + \hat{k}'^{-}k^{+} + k^{-}\hat{k}'^{+} \mid + \rangle,$$

where $|\pm\rangle$ represent the eigen states of the matrix $\sigma \mathbf{B}_0$: $f \mathbf{B}_0 |\pm\rangle = \pm B_0 |\pm\rangle$. Evaluation gives

$$N = (k^{+} + k^{'+}) (k^{-} + k^{'-}) - (k^{'-} - k^{'+}) (k^{+} - k^{-}) \sin^{2}(\chi/2), \tag{3.4}$$

where $k^{\pm} = \sqrt{k^2 \pm B_0}$ and $k'^{\pm} = \sqrt{k^2 - u \pm B_1}$ are the c-numbers now, and χ is the angle between vectors $\mathbf{B_0}$ and $\mathbf{B_1}$. The numerator of (3.2) can be reduced to the form:

$$\hat{A} = k^{-}k^{+} - k^{'-}k^{'+} + \hat{k}^{-}\hat{k}^{'+} - \hat{k}^{'-}\hat{k}^{'+} =$$

$$= k^{+}k^{-} - k^{'+}k^{'-} + (1,'2)(k^{'-} + k^{'+})(\hat{k}^{+} - \hat{k}^{-}) - (1/2)(k^{'+} - k^{'-})(\hat{k}^{-}\sigma \mathbf{b}_{1} + \sigma \mathbf{b}_{1}\hat{k}^{+}),$$

where the first two terms do not contain the σ matrices at all, and b_1 is the unit vector in the direction of B_1 .

Now we are to calculate matrix elements of A

$$\langle \pm | \hat{A} | \pm \rangle = (k^{-} \pm k^{'})(k^{+} \mp k^{'+}) \pm (k^{'+} - k^{'-})(k^{+} + k^{-}) \sin^{2}(\gamma/2),$$

$$\langle \mp |\hat{A}| \pm \rangle = -(k'^+ - k'^-) k^{\pm} \sin \chi.$$

In the case of $\chi = 0$ (and similarly for $\chi = \pi$) the matrix \hat{R} becomes diagonal with the elements:

$$R_{+} = (k^{+} - k^{'+})/(k^{+} + k^{'+}), \quad R_{-} = (k^{-} - k^{'-})/(k^{-} + k^{'-}).$$

For the general case the final expressions for the matrix elements of \hat{R} are:

$$R_{\pm\pm} = \frac{1}{C} \left\{ R_{\pm} \mp \frac{(k'^{+} - k'^{-})(k^{+} + k^{-})}{(k^{-} + k'^{-})(k^{+} + k'^{+})} \sin^{2}(\chi/2) \right\},$$

$$R_{\pm\mp} = \frac{1}{C} \left\{ -\frac{(k'^{+} - k'^{-})k^{\mp}}{(k^{-} + k'^{+})(k^{+} + k'^{+})} \sin\chi \right\},$$

$$C = 1 - \frac{(k'^{+} - k'^{-})(k^{-} - k^{+})}{(k^{-} + k'^{-})(k^{+} + k'^{+})} \sin^{2}(\chi/2).$$
(3.5)

These formulas are useful to calculate the beam splitting, but the notations are not appropriate for an experiment, because both spin states in the incident beam are characterized by the same wave vector $\mathbf{k}^+ = \mathbf{k}^- = \mathbf{k}$ with a given normal component k. Thus, if we consider the splitting of the part of the beam initially polarized along the field, we must replace $k^2 - B_0$ by k^2 which means shifting of all k^2 in (3.5) by $+ B_0$. Thus, \mathbf{k}^+ for that part of the beam becomes, $k^+ = \sqrt{k^2 + 2B_0}$, and $k'^{\pm} = \sqrt{k^2 - u \pm (B_1 \pm B_0)}$. For the part of the incident beam polarized in the opposite direction we must take $k^+ \equiv k$ and then, $k^- = \sqrt{k^2 - 2B_0}$, and $k'^{\pm} = \sqrt{k^2 - u \pm (B_1 \mp B_0)}$.

It is easy to estimate the intensity of reflected beams in the case when the inside field is strong enough to make k'^- be imaginary, and leave k'^+ to be real. In the first approximation with respect to B_0/k^2 the denominator can be replaced by 1, and the intensity of the off-specular beam become proportional to

$$|R_{-+}|^2 = k^2 \left| \frac{-(k'^- - k'^+)}{(k^+ + k'^+)(k^- + k'^-)} \sin \chi \right|^2 = \frac{\gamma B_1 \sin^2 \chi}{2(u + B_1)}, \text{ where } \gamma = \left| \frac{2k}{(k + k'^+)} \right|^2 \approx 1.$$

4. Experiment

The experiment was performed at the time-of-flight reflector leter of polarized neutrons at the IBR-2 reactor in Dubna.

The sample was a thin anisotropic FeCo film on a glass substrate. The external field was applied either parallel to the anisotropy axis in the film plane ($\chi = 0$) or at an angle of

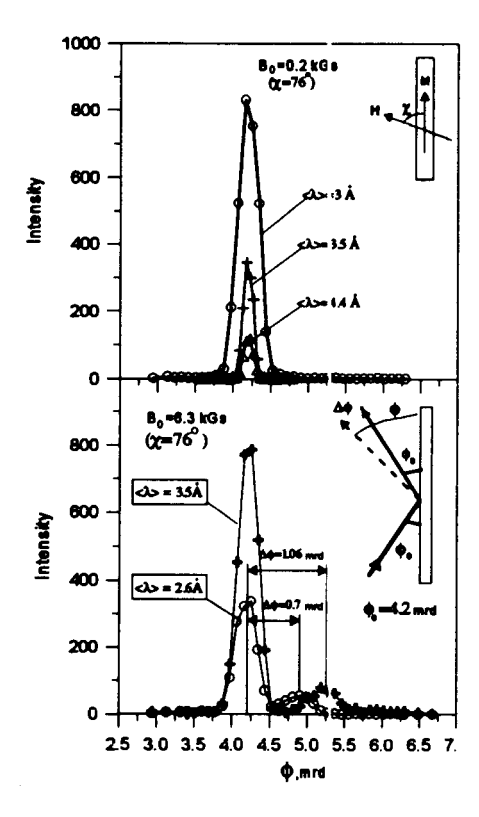


Fig. 3. The dependence of the niflected neutron intensity on the angle ϕ of detector positioning. a) B=0.2 kGs, $\chi=76^\circ$, the detector aperture $\delta\phi=0.18$ mrd, the grazing angle of the incident beam is $\phi_0=4.2$ mrd. The intensity distribution maxima for different λ are observed at the same specular angle $\phi=\phi_0$. b) $\beta=6.3$ kGs, $\chi=76^\circ$, $\delta\phi=0.18$ mrd, $\phi_0=4.2$ mrd. The angular distribution of the reflected intensity for two different intervals of λ . In the vicinity of the specular beam $(\phi=\phi_0)$, offspecular ones appear. The angular shift $\Delta\phi=\phi-\phi_0$ has the quadratic dependence on averaged wavelength $\langle \lambda \rangle$

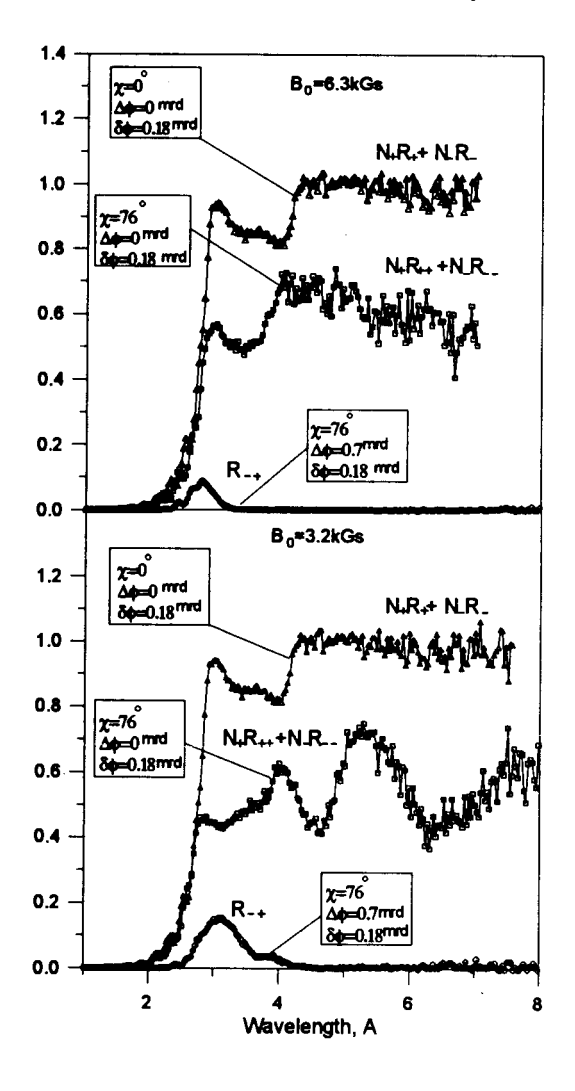


Fig. 4. The wavelength dependence of $N_+R_+ + N_-R_-$ in the specular direction $\phi = \phi_0$ for $\chi = 0$ and $\chi = 76$ deg and of $|R_{-+}|^2$ for $\chi = 76$ deg in the off-specular direction ($\Delta \phi = 0.7$ mrd.). a) B = 6.3 kGs, b) B = 3.2 kGs

0.01 + 7 kGs. The polarized neutron beam with a wide Maxwellian spectrum was incident on the film at a grazing angle $\phi_0 = 4.2$ mrd. The polarization of the beam $P(\lambda)$ was a monotonous function decreasing from P = 0.98 at $\lambda = 1.8$ Å to P = 0.5 at $\lambda = 7$ Å. The detector with a cadmium slit of 0.5 mm width was placed at 2.68 m from the sample. Thus,

the angular aperture of the detector was $\delta \phi = 0.18$ mrd. To determine the reflection coefficients the intensities of the incident and reflected neutrons were measured at different orientation and magnitudes of the external field B.

For $\chi = 0$ the dependence of $N_+R_+ + N_-R_-$ on the wavelength was measured. Here $N_{\pm}(\lambda)$ are proportional to the intensities of the incident neutrons with two spin projections on the external field, and R_{\pm} are the squares of modules of the related reflection amplitudes.

For $\chi=76$ deg, the angular distributions of the reflected neutrons were measured for two magnitudes of the external field: 0.2 and 6.3 kGs (Fig.3). In the field H=6.3 kGs, off-specular neutrons were observed at $\phi>\phi_0$. To determine the dependence of $\Delta\phi=\phi-\phi_0$ on lambda the energy range of counted neutrons was estricted to two intervals $\Delta\lambda_1$ and $\Delta\lambda_2$ around $\lambda_1=2.6$ Å and $\lambda_2=3.5$ Å, respectively. The measured ratio of the magnitudes $\Delta\phi_1(\lambda_1)$ and $\Delta\phi_2(\lambda_2)$ (Fig.3b) satisfies the relation $\Delta\phi_1(\lambda_1)/\Delta\phi_2(\lambda_2)=$ $=(\lambda_1/\lambda_2)^2$ with the precision better than 5%, and corroborates the quadratic dependence of $\Delta\phi$ on λ . The measurements of $\Delta\phi$ at fixed λ and different B corroborate the linear dependence $\Delta\phi\propto B$. For the fixed position of the detector at $\Delta\phi=0.7$ mid and two magnitudes of the external field: B=6.3 and 3.2 kGs the spectral dependence of the square modules of R_{++} , R_{+-} and R_{-+} were measured (Fig.4). The spectral interval of the measurements was determined by the angular detector aperture $\phi=0.18$ mrd. The probabilities $R_{\pm}(\lambda)|^2$ were also measured at $\delta\phi=1.06$ mrd for two magnitudes of the external magnetic field (Fig.5). The position and spectral width of the functions $R_{\pm}(\lambda)$ corroborate the expected theoretical dependence $\Delta\phi\propto B\lambda^2$. It is evident that measurement of nondiagonal elements

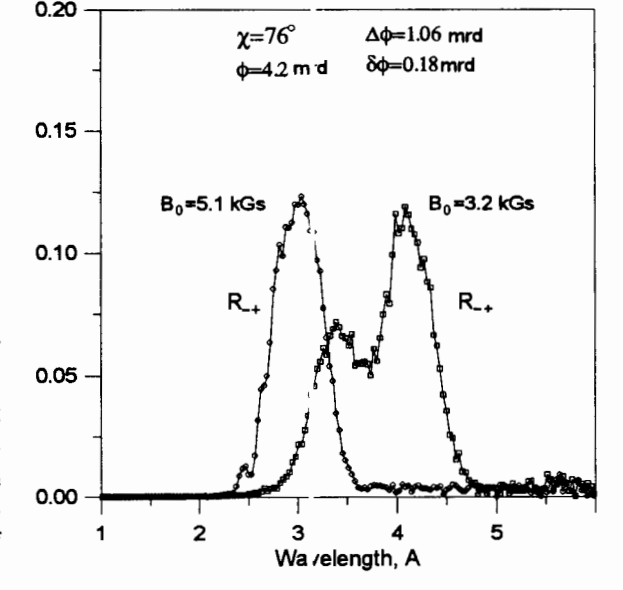


Fig. 5. The dependence of $|R_+|^2$ on λ for $\Delta \phi = 1.06$ mrd and two fields: B = 5.1 kGs, and B = 3.2 kGs. The shift and broadening of the spectral interval for the weaker field corroborate the dependence $\Delta \phi \propto B\lambda^2$. The bell shaped forms of both spectra are related to the small aperture $\delta \phi = 0.18$ mrd of the detector

 $|R_{\pm \mp}(\lambda)|^2$ in a wide spectral interval of λ and in the off-specular direction requires detector with wide angular aperture contrary to the measurement of the sum $N_+R_{++}(\lambda) + N_-R_-(\lambda)$ in the specular direction.

5. Conclusion

The obtained experimental data demonstrate that the reflectometry in high external fields (B > 2 kGs) from noncollinear structures with nondiagonal reflection matrices reveals strong angular dispersion of the reflected neutrons with reversed spins. For the case of nonpolarized incident beam the observation of this dispersion gives the opportunity to measure the nondiagonal elements $R_{\pm \mp}(\lambda)$ in the off-specular beams and the sum $1/2(R_{++}(\lambda) + R_{--}(\lambda))$ in the specular one. It also gives the opportunity to get information on the distribution of magnetization in films using nonpolarized neutrons.

References

- 1. Hughes D.J., Burgy M.T. Phys. Rev., 1951, v.81, p.498.
- 2. Felcher G.P., Hildeke R.O., Crawford R., Haumann J., Kleb R., Ostrowski G. Rev. Sci. Instr., 1987, v.58, p.609.
- 3. Korneev D.A., Pasyuk V.V., Petrenko A.V., Dokukin E.B. Neutron Refectivity Studies on Superconducting, Magnetic and Absorbing Thin Films on the Polarized Neutron Spectrometer at the Pulsed Reactor IBR-2, In: H.Zabel, I.K.Robinson (Eds.) Surface X-Ray Neutron Scattering (Proceedings of the 2nd Int. Conf., Bad Honnef, Germany, June 25—28, 1991, p.213.
- Lauter H.J., Bland J.A.C., Bateson R.D., Jonson A.D. Magnetic Properties of Ultrathin Co/Ag Films Investigated by Polarized Neutron Reflection, Ibid, p.219.
- Endoh Y. In: Neutron Optics Devices and Applications, C.Majkrzak, J.Wood, Editors, Proc. SPIE 1738, 1992, p.224.
- Fitzimmons M.R., Smith G.S., Pynn R., Nastasi M.A., Burkel E. Physica B, 1994, v.198, p.169.
- 7. Ignatovich V.K. Pis'ma ZhETP, 1978, v.28, p.311 (see Sov. JETP Lett.).
- 8. Korneev D.A. Poverhnost', 1989, v.2, p.13 (in Russian).
- Ignatovich V.K. The Physics of Ultracold Neutrons, Clarendon Press, Oxford, 1990.
- 10. Majkrzak C.F. Physica B, 1991, v.173, p.75.
- Korneev D.A., Chemenko L.P. In: Neutron Optics Devices and Applications, C.Majkrzak, J.Wood, Editors, Proc. SPIE 1738, 1992, p.468.
- 12. Zabel H. Physica B, 1994, v.198, p.156.

УДК 575.24: 595.773.4

MOLECULAR CYTOGENETICS OF RADIATION-INDUCED GENE MUTATIONS IN DROSOPHILA MELANOGASTER

I.D.Alexandrov, M.V.Alexandrova, I.L.Lapidus, A.L.Karpovsky

The classical paradigm of spatially unrelated lesions for gene mutations and chromosomal exchange breakpoints induced by ionizing radiations in eukaryotic cells was re-examined in the experiments on the mapping of gamma-ray- or neutron-induced breakpoints in and outside of white (w) and vestigial (vg) genes of Drosophila melanogaster using the in-situ hybridization of the large fragments of the genes under study with the polytene chromosomes of the relevant mutants. The results for the random sample of 60 inversion and translocation breakpoints analysed to date have shown that (i) 50% of them are mapped as the hot spots within big introns of both the genes, and (ii) 21 of 60 breaks (35%) are located outside of genes. It is important to note that 26% (16/60) of the breakpoints analysed are flanked by the deletions, the sizes of which vary from the quarter to a whole of the gene. It was found that the deletions flank both the inversion and translocation breakpoints and arise more often after action of neutrons than photons. An unexpectedly high frequency of the multiple-damaged w and vg mutants that have the gene/point mutation and additional, but separate, chromosome exchange (the so-called double- or triple-site mutants) has shown that the gene ic danger of ionizing radiation is higher than usually accepted on the base of single gene/point mutation assessements.

The investigation has been performed at the Department of Radiation Safety and Radiation Researches, JINR.

Молекулярная цитогенетика радиационно-индуцированных генных мутаций у Drosophila melanogaster

И.Д.Александров и др.

Парадигма классической радиационной генетики о разных «мишенях» для генных мутаций и аберрационных разрывов при наследуемых обменах хромосом в облученных клетках высших организмов экспериментально пока не обоснована, поскольку прямой анализ распределения таких разрывов внутри и вокруг гена до сих тор не был проведен. Восполняя этот пробел, мы проводим такой анализ с помощью метода молекулярной радиоизотопной гибридизации in situ (RIISH) геномных фрагментов двух генов Drosophila melanogaster (w и vg) с политенными хромосомами на большой выборке гамма- и нейтрон-индуцированных мутаций этих генов, цитогенетически ассоц прованных с инверсионными и транслокационными разрывами. Результаты для 60 прознализированных на сегодняшний день таких разрывов показывают, что 1) половина из тих находится внутри изученных генов, кластеризуясь в их больших интронах, 2) 35% (21/60) разрывов расположены за пределами этих генов и 3) 26,6% (16/60) разрывов фланкируют делеции (поте-

ри) части или всего гена. Существенно, что делеции наблюдаются при всех изученных обменах и видах излучения, но чаще после действия нейтронов. Неожиданно высокая частота (35%) комплексных мутантов с точковой мутацией гена и сопутствующим независимым аберрационным обменом (так называемые мутанты с двух-трех-сайтовыми повреждениями на гено и) показывает, что генетическая опасность ионизирующих излучений гораздо выше, чем рассчитываемая сейчас по выходу простых генных мутаций.

Работа выполнени в Отделе радиационной безопасности и радиационных исследований ОИЯИ.

One of the paradigms in the classical radiation genetics claiming that the different and spatially unrelated «targets» or «sites» of initial damage promote the gene mutation and chromosomal break-rejoi ing in eukaryotic cells irradiated by ionizing radiation [1] has not been experimentally substantiated since the direct and systematic analysis of breakpoint distribution in and outside the gene has been not carried out yet. The relationship between gene mutation and breakpoint observed at times on the cytological level has been treated as the «position effect» or as the result of gene damage by the same particle that induces the break in close proximity to the gene [1].

The current version of paradigm that the radiation-induced chromosomal exchange breakpoints were predominantly located within the moderate repeats of DNA neighbouring to gene is founded theoretically [2,3] rather than experimentally since the immediate analysis of the broken repeats and genes has not been performed once again [4].

Thus, the two related and crucial for foundation of paradigm questions as to whether the chromosomal rearrangements with the breakpoints located within the gene are the constituents of the spectrum of gene mutations induced by ionizing radiation and, if so, what are the distribution patterns of breakpoints on the molecular gene maps, remain unresolved as a matter of fact.

To answer questions, the spectrum of gene mutations induced by gamma-rays (5—40 Gy) or fission neutrons (2.5—20 Gy) at the white (w^+) and vestigial (vg^+) genes of Drosophila melanogaster was at first studied by the conventional genetic and cytological analysis. Using of the genes which are differring from each other in both the fine exone-introne structure and the location in genome (Fig.1) permits the general and gene specific features to be ascertained in the action of radiation on the gene level.

According to the data obtained to-date, one of the general conclusions based on the results for the two genes studied is that the spectrum of gene mutations for any Drosophila gene damaged by low- or high-LET radiation consists of the three main subclasses: (i) cytologically point mutations, (ii) single- or multi-locus deletions and (iii) exchange mutations (inversions, transpositions, translocations) with gene specific phenotype. The last come to almost the third of all radiation-induced heritable gene alterations [5,6].

Therefore, the chronosomal exchanges modifying the gene expression are the important and constant part of spectrum of gene mutations induced by different quality radiation. What are the distribution patterns of the chromosomal breakpoints for the exchanges score?

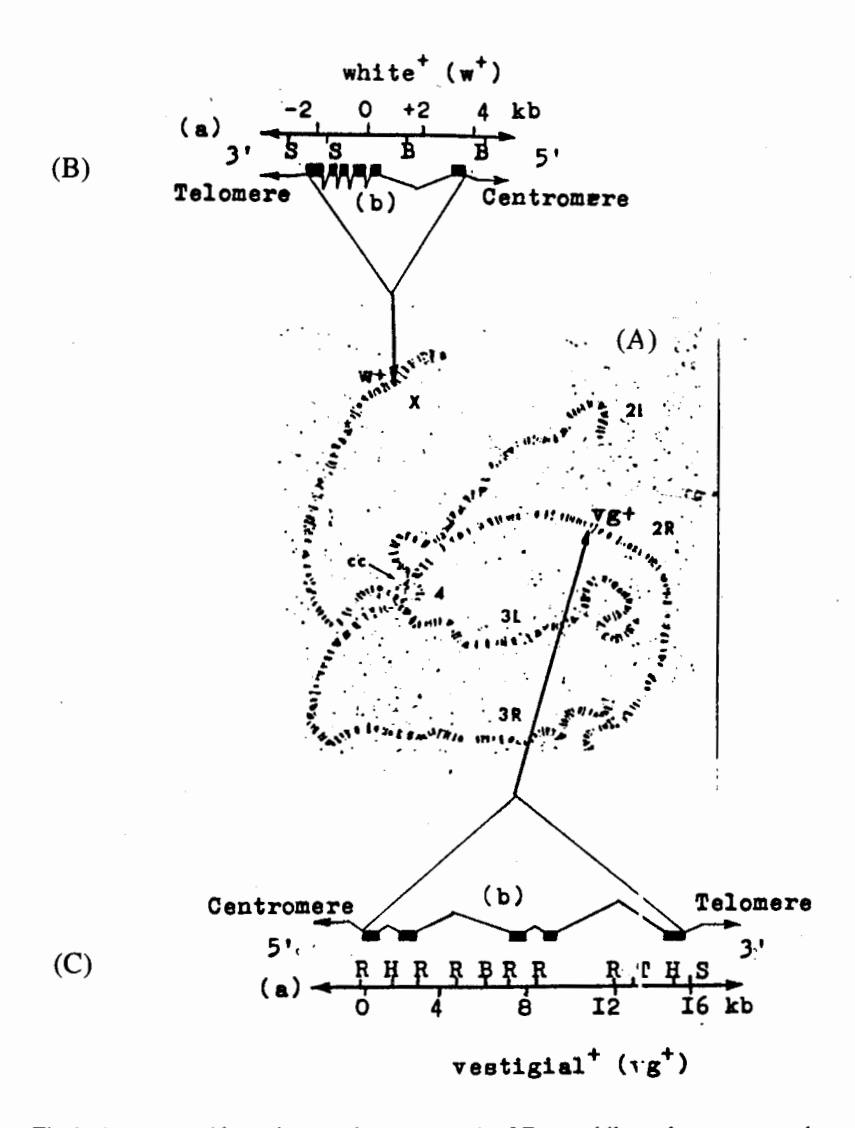


Fig.1. A genome (the polytene chromosomes) of Drosophila melanogaster and localization of w^+ (X chromosome) and vg^+ (2R chromosome) genes (A). (a) and (b) denote the schemes of the physical maps (in kb = 1000 base pair of DNA) and the fine exon (black boxes) — intron (broken lines) structures, respectively, for w^+ (B) and vg^+ (C) genes

The cytological analysis of the mutant w and vg polytene chromosomes has shown that each of the genes recombinates to form exchange with the specific sites of its own or heterogenous chromosome to give rise to the inversions and transpositions or the translocations, respectively (Fig.2a,b and Fig.3a,b). However, the second breakpoint of the ex-

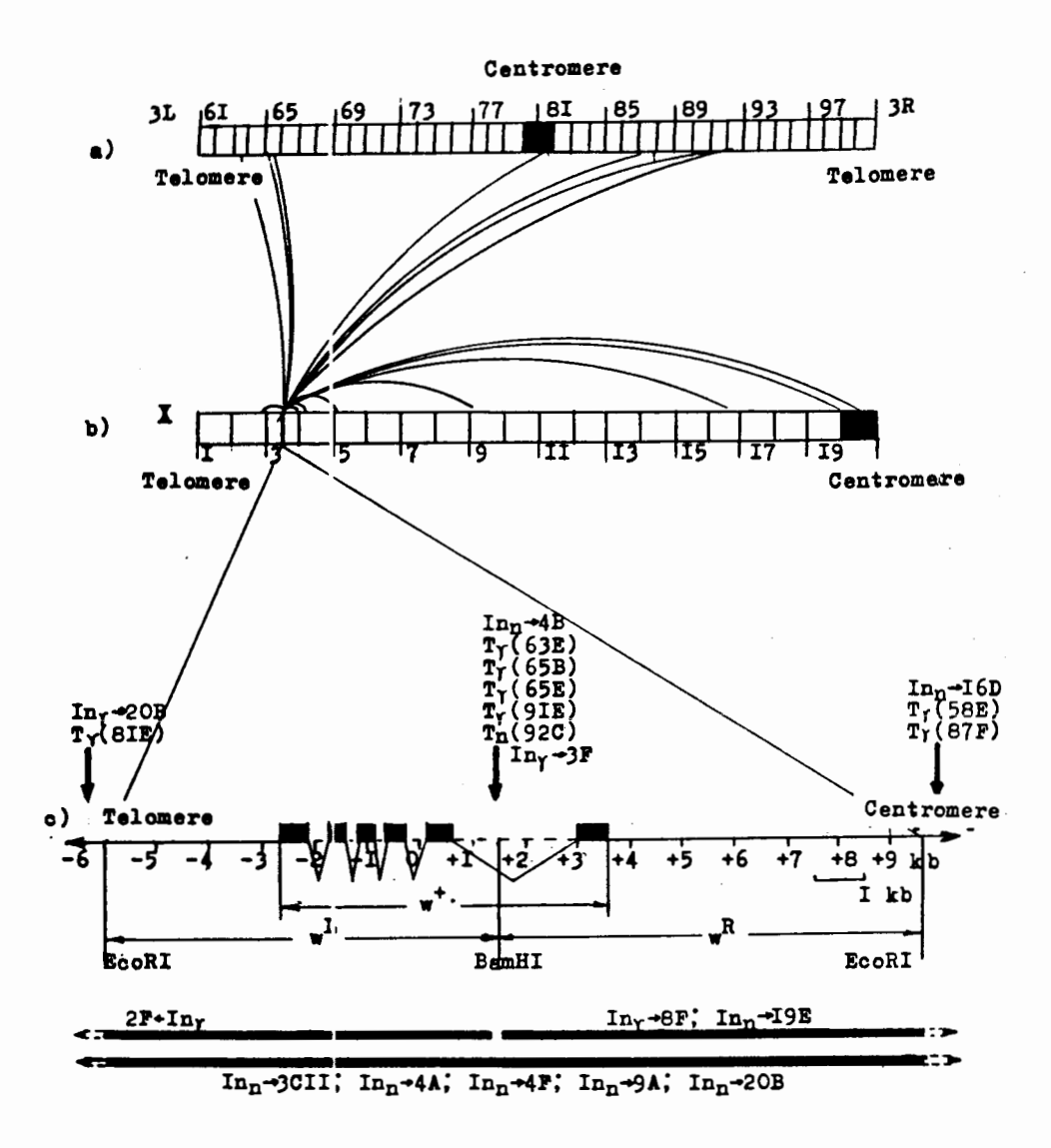


Fig. 2. Genomic (a and b) and intragenic (c) localization of the chromosomal exchange breakpoints underlying the inversions (In and translocations (T) induced by gamma-rays (γ) or neutrons (n) in Drosophila sperms and scored as the w gene mutations. (a) and (b) denote the schemes of the third and X polytene chromosomes, respectively. (c) showes the physical map of 6 kb w^+ gene and adjacent regions covered by w^L and w^R fragments with the relevant EcoRI and BamHI sites, exons (black boxes) and introns (broken lines). The location of the breakpoint «hotspote» is depicted by the black arrows. The sizes of deletions accompanying the breakpoints are shown by the black boxes below the map. The genomic sites with which the w gene interacts are noted by the thin arrows (for inversions) or the numbers w th letter in parentheses (for translocations).

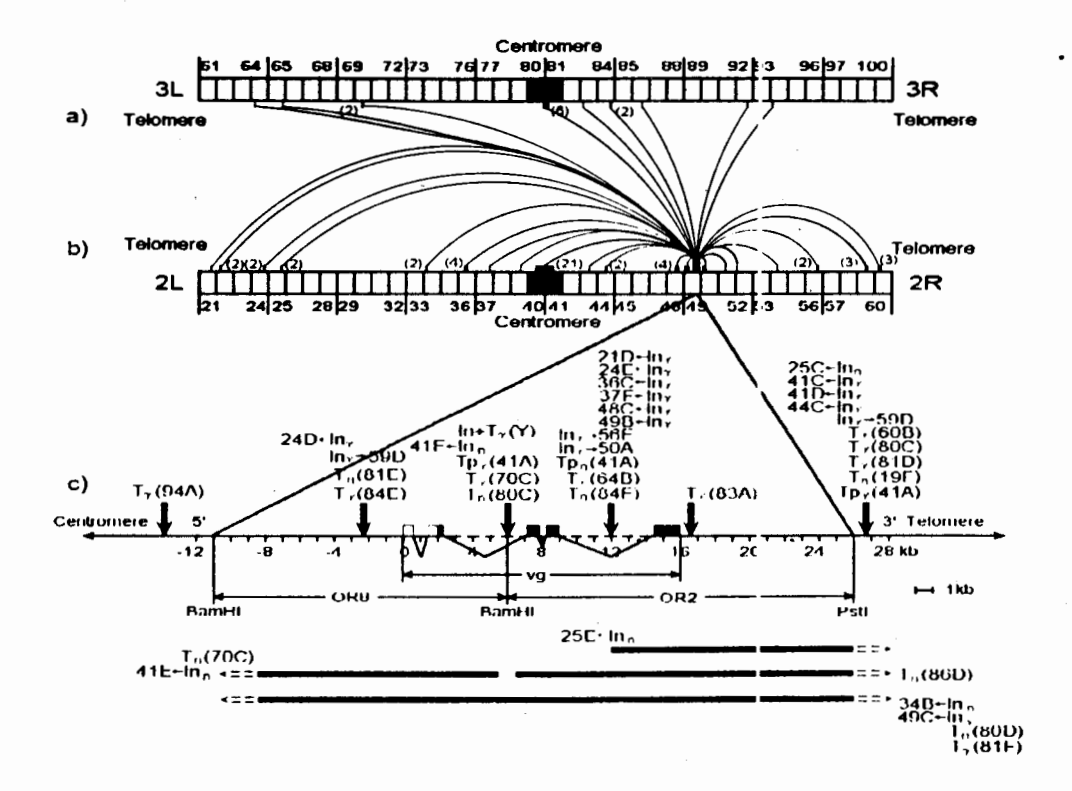


Fig. 3. Genomic (a and b) and intragenic (c) localization of the chromosomal exchange breakpoints underlying the inversions (In) or transpositions (Tp) and translocations (T) induced by gamma-rays (γ) or neutrons (n) in Drosophila sperms and scored as the vg gene mutations. (a) and (b) denote the schemes of the third and second polytene chromosomes, respectively, he «hotspots» on which were shown by the numbers in parentheses (the amount of independent hits for given site). (c) shows the physical map of 16 kb vg gene and adjacent regions covered by OR8 and OR2 fragments with the relevant BamHI and PstI sites. For all the rest designations see Fig.2

changes was found to be closely associated always with the sites of cytological localization of the genes under study (3C2.3 band for w^+ , Fig.2b and 49D3 pand for vg^+ , Fig.3b).

Since such breakpoints are accompanied by the gene-specific phenotypes it may be presumed, if the classical notions are bearing in mind, that these breaks are lying in close proximity to the genes and the mutant phenotypes were brought about by «position effect» or by direct gene lesions accompanying the chromosomal breaks.

To detect precisely the position of the breakpoints around the genes of interest, the state of gene structures and of their neighbouring sequences was studied by in situ radioactive isotope hybridization technique (RIISH) [7] and using the sets of gene fragments covering the genes and adjacent sequences (Fig.2c and Fig.3c). In particular the cloned in pUCI9 distal $(L^+, 7.5 \text{ kb})$ EcoRI-BamHI and proximal $(R^+, 8.0 \text{ kb})$ EamHI-EcoRI fragments of

genomic DNA covering the w^+ gene and the 3.5 kb DNA stretches from each side of this gene were used for analysis of the exchange w mutants, and the cloned in EMBL3 proximal (OR8, 16.5 kb) and distal (OR2, 21.5 kb) genomic fragments of the vg^+ locus were employed for analysis of the vg re-arrangements. It is of importance to note that the couples have got the BamHI sites in common lying in the big introns of the genes (Fig.2c and Fig.3c). When using these tagged fragments we have suggested that localization of the whole fragment or its parts visualized as hybridization site at full intensity or labeled sites at less than half full intensity, respectively, on the mutant polytene chromosome will be determined by a seat of breakpoint in or outside the gene.

The data for the 60 w and vg exchanges examined to-date show that 35% (20/60) of them have the breakpoints ocated outside the genes under study (Fig.2c and Fig.3c). Therefore, the w and vg phenotypes for a large proportion of cytologically visible exchanges are not directly founded by the breaks and seem to result from the «position effect» or independent damage of gene. To choose between these alternative explanations, the relevant experiments are under way.

A new and important finding is that more large part of the exchanges studied (50%) have the breakpoints lying inside both the genes since the transferences of any whole fragment (the breaks are passing through the big introns near BamHI site) or only unequal parts of OR2 (the breaks are located in the second big intron of the vg gene) are observed in such cases.

These results show that although the initial (preaberration) lesions were distributed by a chance through the gene volume only those of them which are situated in the certain («target») intron sequences have a high likelihood to be realized as the chromosomal exchange breakpoints. The s udy of the molecular nature of these «targets» is an important task in hand for our researches.

Other new and important result of the work performed is that a considerable part (26.6% or 16/60) of the v and vg exchanges analysed is found to be the mutants the breakpoints of which are accompanied with the molecular deletions of varying sizes (7-38 kb) or even more) (Fig.2c and Fig.3c). Thereby, as is seen, all partial deletions are begining within the big introns also. It is of importance to note too that the deletions accompany both the inversion and translocation processing independently of quality radiation, but more frequently after action of neutrons.

Thus, the results outlined above enable one to note the following new molecular features of exchange processing in the irradiated eukaryotic cells: (i) the exchange breakpoints are regularly located within a gene; (ii) the breaks are clustered within the certain and relatively short sequences of the big introns, and (iii) almost the third of breaks are flanked by the molecular deletions the sizes of which vary from 7 to 38 kb (i.e., the whole gene).

Among the others two our findings require some comments. Firstly, the exchange break/deletion combination (each of them are usually independent events) shows that the radiation-induced chromosomal exchanges are formed by more complex mechanism than one based on the genetic recombination as such [8]. Our data allow the suggestion to be

made that such exchanges are promoted by the local clustered and recombinogenic damages over several topologically drawn closer to one another chromat n molecules with subsequent mis-rejoining by «illegitimate» recombination either «slippage» or by both the processings, simultaneously. The increase of severity of DNA-related damage, for example, after action of high-LET radiation must rise both the likelihood of deletion formation and its size that is really observed in the experiments with neutrons (Fig.2c and Fig.3c). The sequencing of DNA at the exchange breakpoints without the deletions detected by RIISH technique should answer the important question as to whether the deletions attend any radiation-induced break-rejoining processing.

Secondly, the data obtained for the two genes studied show hat exchange breakpoints are often situated outside the gene and accompanied nevertheless by gene inactivation. This inactivation for gene which was transferred to centromeric heterochromatin (euchromatin—heterochromatin rejoining) may really result from the «position effect» [9] (it is all our cases where the genes under study recombinate with the 9, 40, 41, 80 and 81 heterochromatic regions of the polytene chromosomes, Fig.2a,b and Fig.3a,b). However, this effect is not typical for euchromatin-euchromatin rejoin ng [9]. Therefore, gene inactivation in such exchanges (all our the rest cases) is obviously broght about by independent point (?) damage of gene itself. Thus, the genome of such mutants containes two (or more) heritable mutations simultaneously (the so-called complex or double, triple, etc., mutants).

The property of ionizing radiation to induce such complex mutants proportionally to dose has been already noted earlier on the base of cytological [10] and genetical [11] data. Confirmation of these observations on the molecular level is another important result of our work which has had a great theoretical and applied significance showing that a new approaches need to assess the genetic risk of ionizing radiation the genetic danger of which is proved to be higher than accepted on the base of single gene/point mutation assay.

Acknowledgments

This work was partly supported by grant from Russian State Program «Frontiers in Genetics» and grant 96-04-50741 from RFFR.

References

- Lea D.E. Actions of Radiation on Living Cells. Cambridge, University Press, 1946.
- 2. Soyfer V.N., Akifyev A.P. J. General Biol. (Rus.), 1976, v.37, p.854.
- 3. Nemtseva L.S., Romanov V.P. Progr. Curr. Genet. (Rus), 1980, v.9, p.3.
- 4. Lefevre G.Jr. Cold Spring Harber Symp. Quant. Biol., 1974, v.38, p.591.
- 5. Alexandrov I.D., Alexandrova M.V. Drosophila Inform. Service, 1987, v.66, p.185.
- 6. Alexandrov I.D., Alexandrova M.V. Doklady Acad. Sci. USSR, 1990, v.315, p.484.
- 7. Pardue M.L. et al. Chromosoma, 1970, v.7, p.1.

- 8. Akifyev A.P. Physiol. General Biol. Rev., 1995, v.10, p.1.
- 9. Hannah A. Adv. in Genetics, 1951, v.4, p.87.
- 10. Dubinin N.P., Hvostova V.V., Mansurova V.V. Doklady Acad. Sci. USSR, 1941, v.31, p.386.
- 11. Alexandrov I.D. Mutation Res., 1984, v.127, p.123.